1960

Spectrographic investigation of a plasma jet

Booth, Roger G.; Albers, William P.

Monterey, California: U.S. Naval Postgraduate School

SPECTROGRAPHIC INVESTIGATION OF A PLASMA JET

ROGER G. BOOTH
and
WILLIAM P. ALBERS

SPECTROGRAPHIC INVESTIGATION OF A PLASMA JET

Roger G. Booth

and

William P. Albers

SPECTROGRAPHIC INVESTIGATION

OF A PLASMA JET

by

Roger G. Booth
Lieutenant, United States Navy

and

William P. Albers
Lieutenant, United States Navy

Submitted in partial fulfillment of
the requirements for the degree of

MASTER OF SCIENCE
IN
AERO-PHYSICS

United States Naval Postgraduate School
Monterey, California

1960

SPECTROGRAPHIC INVESTIGATION OF A PLASMA JET

by

Roger G. Booth

and

William P. Albers

This work is accepted as fulfilling

the thesis requirements for the degree of

MASTER OF SCIENCE

IN

AERO-PHYSICS

from the

United States Naval Postgraduate School

ACKNOWLEDGEMENTS

The authors wish to express their gratitude to Dr. Richard M. Head, for suggesting the problem and his continued guidance and encouragement; Dr. Gunter Ecker for his helpful suggestions and criticisms; and to Professor Sidney H. Kalmbach for his help with the spectrograph.

The authors wish to thank Mr. Robert Smith for his assistance in the instrumentation build-up and technical advice on electronics problems.

TABLE OF CONTENTS

LIST OF ILLUSTRATIONS

Figure

Table

1. INTRODUCTION

The electric arc, which has been known for over fifty years, appears at first glance to be a simple mechanism. However, investigations of the arc have proved its complexity and the difficulty in applying theory to reality. In Ecker's[1] discussion there are listed over 500 articles concerning the arc.

A descendant of the electric arc is the relatively new plasma or arc jet which is even more complex. The plasma or arc jet consists of an electric arc confined and stabilized by a swirling vortex of gaseous or fluid media. In confining the arc, the current density and temperature are increased causing a partial ionization of the surrounding media and thus forming a plasma which is defined very generally as a system of charged and neutral particles. The plasma is then passed through a nozzle. The physics of the ionized portion are treated fully in the literature.[2,3] If the plasma is further stabilized with magnetic fields, the theory comes under the title of magnetohydrodynamics[4], a development of the past few years.

With the advent of space travel and high Mach number flight, the plasma jet is a natural tool for investigations into high enthalpy flows by aerodynamists and other interested parties. When used for research in these areas, one of the parameters that requires determi-

[1]G. Ecker, Current Transition Gas-Metal, I. Electrode Discharge Components of the Arc, Technical Report FTR-1, Institute Fur Theoretische Physik Der Universitat Bonn, Bonn, Germany, 1959.

[2]L. Spitzer, Jr., Physics of Fully Ionized Gases, Interscience Publishers, Inc., New York, 1956.

[3]W. P. Allis, Motions of Ions and Electrons, Handbuch der Physik, Band XXI, Gas Discharges I, S. Flugg (Ed.), Springer-Verlag, Berlin, Gottingen, Heidelberg, 1956.

[4]T. G. Cowling, Magnetohydrodynamics, Interscience Publishers, Inc., New York, 1957.

nation is temperature. Here a problem arises because normal methods of temperature measurement (e.g. thermocouples, etc.) fail.

Indirect methods of temperature measurement are available and one of these, spectrographic means, offers several possibilities for temperature determination. Two of these possibilities are:

a. Molecular band spectra intensity distribution[5].

b. The Stark broadening of plasma line spectra [6,7].

The purpose of this paper, then, is to investigate the practicality of these methods for the U. S. Naval Postgraduate School plasma jet, as Kantrowitz[8] and Seay[9] have done with shock tubes.

[5]G. Herzberg, Spectra of Diatomic Molecules, D. Van Nostrand, Inc., New York, 1934.

[6]H. E. White, Introduction to Atomic Spectra, McGraw-Hill Book, Inc., New York, 1934.

[7]H. A. Bethe and E. E. Salpeter, Quantum Mechanics of One and Two Electron Atoms, Academic Press Inc., New York, 1957.

[8]Petschek, Rose, Glick, Kane, and Kantrowitz, J, Appl. Phys. 26, 83 (1955).

[9]G. E. Seay, The Visible Radiation from Helium in a Strong Shock Wave, LAMS-2125, Los Alamos Scientific Laboratory, New Mexico, 1957.

2. EXPERIMENTAL SET-UP

In this section only a brief outline will be given for the experimental procedure and apparatus. For those more interested in the technical aspects and the difficulties experienced in instrumentation, the Appendix contains complete coverage of these and related matters.

The plasma jet at the U. S. Naval Postgraduate School was developed for use with direct current power inputs up to several megawatts. The physical makeup of the plasma jet, Fig. 1, consists of a cylindrical body made of aluminum with an inside diameter of four inches. The body is mounted vertically on a movable stand. Concentric with the barrel and passing through the bottom of the stand is the cathode holder mounted on a racking screw to provide vertical motion for arc gap adjustment. The top contains a de Laval nozzle which also functions as the arc anode. Both electrodes have replacable inserts made of either carbon or tungsten. A window of either pyrex or sapphire was used to observe the arc. Arc stabilization can be provided by the introduction, tangentially, of water or gas. This investigation was made entirely with gaseous media. In addition, water cooled pancake coils can be added inside the barrel to provide magnetic stabilization. The variation of input power is made possible by the variable gap spacing, the external resistance, and the supply voltage. The complete mechanical and electrical characteristics of this particular plasma jet are discussed by Gates and Thomas[10].

The voltage, current, and pressure in the arc body were measured and were displayed by Edin pen recorders. An interesting method was

[10]Gates and Thomas, Plasma Jet Electrical Characteristics, U. S. Naval Postgraduate School Thesis, 1959.

used to measure currents up to 4000 amps -- a magnetic saturable reactor circuit (transductor) was used to transform the direct current of the line into a signal that does not require large scale ammeters.

Spectrograms of the arc were made with a 3 meter grating (15,000 lines/inch) Eagle mount spectrograph manufactured by Baird Atomic. The inverse dispersion in the first order is 5.42 A/mm. The spectrograph camera covers a range of approximately 2500 A. An alternate to the camera is a direct reader head which measures spectural line intensity directly using photomultiplier tubes.

The schematic of Fig. 2 shows the relative positioning of the components involved and the light path from the arc to the spectrograph. Fig. 3 shows the parabolic and plane mirrors used to direct the light from the plasma jet to the entrance slit at the left. The arc was also imaged on a screen where it was observed magnified approximately 12X and slow motion color movies were obtained.

The experimental data was obtained by varying the power input to the arc and introducing either argon, helium or nitrogen into the arc. Spectrograms were taken of the plasma spectra; argon and helium giving line spectra and nitrogen the cyanogen (CN) band spectra when carbon electrodes were used.

3. MOLECULAR SPECTRA

The intensity of an emitted spectral line from an ensemble of radiating emitters depends on the population of emitters present in the initial energy level concerned in the transition and the probability of the transition occuring. The intensity of a line emitted by a molecular source is defined as the energy emitted by the source at the frequency of the line and is given by[5]

$$I_{nm} = N_n \, hc \, \nu_{nm} \, A_{nm} \qquad (3\text{-}1)$$

where

N_n = number of molecules in the initial energy level E_n

h = Plank's constant

c = velocity of light

ν_{nm} = wave number of emitted line

A_{nm} = transition probability of the transition from energy level E_n to energy level E_m and called the Einstein transition probability of spontaneous emission.

The term $hc\nu_{nm}$ is the energy of each light quantum of wave number ν_{nm}.

The relations for the Einstein transition probability and the energy level population can be obtained from the literature[5,11]. Combining these relations into the intensity equation, the formulation becomes

$$I_{nm} = \frac{C}{Q_r} \, g_n \, \nu_{nm}^4 \, \exp - E_n/kT \qquad (3\text{-}2)$$

[11] Duffendack and LaRue, J. Optical Soc. Amer., 31, 146, 1941.

where the undefined factors are

C = constant depending on the change in dipole moment and total number of molecules in the initial level

Q_r = state sum or partition function

g_η = statistical weight or degeneracy of the level η

k = Boltzman constant

T = absolute temperature

The characteristics of band spectra are described by electronic, vibrational, and rotational transitions in a molecule. For a diatomic molecule the total energy of a given level, then, can be ascribed components corresponding to electronic, vibrational, and rotational levels. Assuming that thermal equilibrium exists within the arc, then one of the modal temperatures of the electronic, vibrational, or rotational excitations can be used to express the media's temperature. The assumption of thermal equilibrium at atmospheric pressure and above seems reasonable in view of the results of several investigators[12,13] using carbon arcs.

Within the band spectra intensity method there are several alternatives for temperature determination most of which require tedious spectrographic plate calibration. One, however, originated by Knauss and McCay[14] and used by Greenshields[15] eliminates this requirement.

The spectral lines within the band, Fig. 4, are the result of the rotational transitions. Each of the rotational energy levels is

[12] J. S. Smit, Physicia, XII, 683, 1946.
[13] Ornstein and Brinkman, Proc Roy. Acad. Amsterdam, XXXIV, 33, 498, 1931.
[14] Knauss and McCay, Phys. Rev., 52, 1143, Second ser., 1937.
[15] D. H. Greenshields, NASA TN D-169, 1959.

assigned a rotational quantum number, J; the statistical weight, g_η, and the initial energy level, E_η, of 3-2 can be written in terms of these quantum numbers. Thus the intensity equation becomes

$$I = \frac{C}{Q_r} \nu^4 (J' + J'' + 1) \exp - \left[\frac{B_{v'} J'(J'+1) hc}{kT} \right] \quad (3\text{-}3)$$

where

J' = upper energy level quantum number

J" = lower energy level quantum number

$B_{v'}$ = rotational constant

Considering any one band of the spectrum the term $\frac{C\nu^4}{Q_r}$ is nearly constant. Quantum mechanics assigns a selection rule $\Delta J = \pm 1$ to the rotational transitions. As a result, there are two series of lines, called branches inside the band. These are seen as paired lines in Fig. 4. The $\Delta J = +1$ defines the P branch and $\Delta J = -1$ defines the R branch. These branches and associated quantum numbers are shown in Fig. 5, which is a microdensitometer tracing of Fig. 4. Making the proper substitution for the selection rule, the intensity for each branch is then

$$I_P = \frac{2C\nu^4}{Q_r} (J_P + 1) \exp - \left[\frac{B_{v'} J_P (J_P - 1) hc}{kT} \right] \quad (3\text{-}4)$$

$$I_R = \frac{2C\nu^4}{Q_r} J_R \exp - \left[\frac{B_{v'} (J_R + 1)(J_R + 2) hc}{kT} \right] \quad (3\text{-}5)$$

Knauss and McCay[14] noted that the intersection of the envelopes

of the intensities of the P and R branches varied with temperature. The conditions required at this intersection are

$$\nu_P = \nu_R \tag{3-6}$$

$$I_P = I_R \tag{3-7}$$

Then solving for temperature from 3-4, and 3-5 using 3-6 and 3-7, the formulation is

$$T = B_{v'} \frac{hc}{k} \left[\frac{J_P(J_P-1) - (J_R+1)(J_R+2)}{\ln (J_P+1)/J_R} \right] \tag{3-8}$$

where J_P and J_R are the values at the envelope intersection. A pyrometric curve of temperature vs J_P and J_R may be constructed, Fig. 6, if the values of the quantum numbers are known. These values can be obtained from a Fortrat diagram, Fig. 7, an excerpt of the complete Fortrat parabola (found in the literature for the various bands as a table[5,16,17] or a formula[5]) which relates J_P and J_R to wave number.

The technique, then, consisted of exposing spectrographic plates to the $0 \longrightarrow 1$ band at 4216 A of CN. The spectrogram is then traced with a microdensitometer, Fig. 5. The lines of the tracing are assigned the proper branch rotational quantum numbers from Fig. 7 and envelopes of the branch intensities drawn, Fig. 5. The intersection quantum number is used as an entry into the pyrometric curve, Fig. 6, for temperature. The experimental results obtained from various runs of the arc jet using nitrogen gas are:

[16] Smit-Miesser and Spier, Physicia, IX, 193, 1942.
[17] Spier and Smit, Physicia, IX, 597, 1942.

Power (kw)	Temperature (°K)	
22.8	5200	
24.8	5140	
30.4	5300	
38.2	4990 - 2 runs	
41.5	5300	
54.0	5300	
63.0	- -	eliminated due to poor plate exposure
85.5	above 5600	

On one run the expanding portion of the deLaval nozzle was removed and a spectrogram taken of the area adjacent to, and downstream of the carbon anode insert. The experimental temperatures obtained are:

a. 4680°K at a position near the anode

b. 4320°K at a position approximately 0.2 inches above a.

4. LINE BROADENING IN PLASMA RADIATION

The important causes of line broadening in a plasma may be listed as follows:

a. Natural width

b. Doppler broadening

c. Coulomb interactions (Stark effect)

A. Natural width

The natural width of a line may be calculated in two ways.[6] From a classical approach, one may expand the damped oscillations from a radiating electric charge in a Fourier series. One then obtains the Lorentz shape:

$$I(\omega) = \frac{\omega_{1/2}}{2\pi} \quad \frac{1}{(\omega_o - \omega)^2 + \left(\frac{\omega_{1/2}}{2}\right)^2} \qquad (4\text{-}1a)$$

where:

$\omega_{1/2}$ = full width at half intensity.

$$= \frac{2}{3} \quad \frac{e^2 \omega_o^2}{m c^3}$$

Or, in terms of wavelength, this becomes:

$$\Delta\lambda = \frac{\lambda^2 \Delta\omega}{2\pi c}$$

$\Delta\lambda$ = constant = $1.16 \cdot 10^{-4} A$

From quantum mechanics one also obtains the Lorentz shape for the probability distribution of the term value for an energy state. This results in an intensity distribution for a transition between two states of:

$$I(\omega) = \frac{\omega_{1/2} + \omega'_{1/2}}{2\pi} \quad \frac{1}{(\omega_o - \omega)^2 + \left(\frac{\omega_{1/2} + \omega'_{1/2}}{2}\right)^2} \qquad (4\text{-}1b)$$

where $\omega_{1/2}$ and $\omega'_{1/2}$ are the half widths of the upper and lower states. This yields the classical result for a mean lifetime of about 1.6×10^{-8} sec., which is a typical value for optical transitions.

B. Doppler broadening.

The classical and quantum mechanical treatment yield the same result for Doppler frequency shift, namely:

$$\frac{\Delta\nu}{\nu_0} = \frac{u}{c} \qquad (4\text{-}2)$$

where: $\Delta\nu$ = frequency shift

ν_0 = stationary frequency

u = component of velocity in the direction of observation

c = velocity of light

Assuming a Maxwellian distribution of velocities for the radiating atoms, the probability (dw) that the velocity will lie between u and u + du is:

$$d(\omega) = \sqrt{\beta/\pi}\ \exp -\left[\beta u^2\right]\ du \qquad (4\text{-}3)$$

where: $\beta = \mu/2RT$

μ = molecular weight

Substituting the value of u from 4-2 into 4-3 we obtain

$$I(\nu) = \text{const.}\ \exp -\left[\beta \frac{c^2}{\nu_0^2}(\nu - \nu_0)^2\right]$$

Solving for the half intensity width we find:

$$\frac{\omega_{1/2}}{\omega_0} = \frac{\Delta\lambda}{\lambda_0} = 1.67\sqrt{\frac{2RT}{\mu}} \qquad (4\text{-}4)$$

For helium at 20,000 ^{o}K this is:

$$\frac{\omega_{1/2}}{\omega_o} = 5.07 \times 10^{-5}$$ which is negligibly small compared with the other half widths considered below.

C. Charged particle interactions

Coulomb interaction as manifested in the Stark effect is considered to be the principle broadening agent in a plasma. Dipole, quadrupole, and Van der Waal's interactions are negligible in comparison with coulomb effects. The Stark effect on a radiating atom in a plasma is particularly difficult to treat because the fields are large and are time dependent, both in magnitude and direction, due to the motion of the charged particles.

A typical value is Holtzmark's most probable field:

$F_o = 3.9\ e\ n_e^{2/3}$, which, for $n_e = 10^{18}$ cm^{-3} is:

$= 560$ KV/cm

This is larger by a factor of two than the usual homogeneous field used in the laboratory to study the Stark effect.

(1) Statistical theory.

Among the various approaches to the problem of Stark broadening, the semi-classical Holtzmark theory[18] is the oldest and has met with the most success in the past. Holtzmark treats the broadening as if it were the sum of Stark shifts caused by the probability distribution of ions around the radiating atom. He neglects, however, the Gibb's free energy which accounts for the reduced probability of having a high ion density in configuration space. Ecker[19]

[18] J. Holtzmark, Ann. Physick 58, 577 (1919)
[19] G. Ecker, Z. Physik 148, 593, (1957)

considers the Gibb's energy through the Debye-Hückel screening mechanism which introduces effects due to electrons. He finds a considerable deviation from the Holtzmark theory for small values of the parameter:

$$\delta = \left(\frac{4\pi D^3}{3}\right) \frac{1}{n_e} ,$$

where D = Debye length,

which is just the number of ions within the Debye sphere. Margenau[20] presents the statistical theory on the basis of the quantum mechanical "adiabatic hypothesis" and proves the following two theorems:

(a) The statistical theory is always applicable in the far wings of a line, i.e. far from the unperturbed frequency.

(b) If a spectral line is broadened by single impacts and it is the time during which a passing particle moves a distance equal to the impact parameter ρ, then the statistical theory is applicable if:

$$\omega_{1/2} \, \Delta t >> 1 \qquad (4\text{-}5)$$

where $\omega_{1/2}$ = measured half width of the line

If one takes d/2 for an estimate of ρ where $d = (1/n_e)^{1/3} = 10^{-6}$cm, T = 20,000 °K, and $\omega_{1/2} = 5 \times 10^{12}$ sec^{-1}, then we find:

$\omega_{1/2} \Delta t$ = 0.25 for electrons

= 15 for He ions, neither of which satisfy condition 4-5.

The adiabatic hypothesis requires an integral containing "resonance" terms $1/E_1 - E_k$ (where the E's are term values) to be small. Thus adiabati-

[20] Margenau and Lewis, Revs. Modern Phys. 31, 572, (1959)

city will not hold for atoms with small energy level separations (degeneracy or near degeneracy). Note that the theorem b. above requires the perturber to have a classical path, which is not justified for electrons in some cases.

(2) Impact theory.

Impact theory, in general, makes use of the adiabatic hypothesis above and also the "sudden" approximation:

$$\omega_{1/2}\,\Delta t << 1 \qquad (4\text{-}6)$$

However, using the above values (which are typical for this experiment) it is seen that this relation is not satisfied either. The impact theory has been developed by Lindholm[21] and is presented by Margenau[20] using recent stochastic methods. The theory essentially formulates the intensity profile in terms of sudden, binary changes in the phase of the radiation. A graphical integration was performed by Margenau to evaluate the numerical factors. His results are:

a. Half width (Lindholm)

$$\omega_{1/2} = 11.4\ \Omega_4^{2/3}\, v^{1/3}\, \eta_e \qquad (4\text{-}7a)$$

This may be transformed into a more tractable result as follows. Margenau[20] shows that the quadratic Stark coefficient may be approximated by:

$$\Omega_4 = \frac{1}{2}\left(\frac{n}{Z}\right)^6 \frac{a^3 e^2}{\hbar}$$

[21] E. Lindholm, Arkiv Mat. Astron. Fysik, 28B, No. 3, (1941)

where n = principle quantum number

z = ionic charge number

a = first Bohr orbit = 5.2917×10^{-9} cm

v = speed of perturbing particle in the center of mass coordinate system. For helium, the above parameters may be solved for

$$\Omega_4 = 1.62 \times 10^{-17} n^6$$

From kinetic theory and assuming a Boltzman velocity distribution we find, in the center of mass system:

$$\frac{1}{2} \mu v^2 = \frac{3}{2} kT$$

where μ = reduced mass of the perturber

For He^+ ions then:

$$\mu = 3.323 \times 10^{-24} \text{ gm}$$
$$v^{1/3} = 106.33\, T^{1/6}$$

where T is expressed in electron volts. Substituting the above values into 4-7a we obtain:

$$\omega_{1/2} = 7.75 \times 10^{-9} n^4 n_e T^{1/6} \text{ (sec}^{-1}\text{)} \qquad (4\text{-}7b)$$

b. Shift (Lindholm). Margenau's result for the shift of the intensity maximum is

$$\delta = 9.8\, \Omega_4^{2/3} v^{1/3} n_e \qquad (4\text{-}8a)$$

which may be transformed exactly as above to:

$$\Omega_4 = 6.66 \times 10^{-9} n^4 n_e T^{1/6} \text{ (sec}^{-1}\text{)} \qquad (4\text{-}8b)$$

(3) Quantum mechanical treatment of electron effects.

Kivel, Bloom, and Margenau[22] (KBM) apply quantum mechanics from the outset to the effects of electrons on plasma radiations. They describe three mechanisms: a. Universal broadening (γ_u) as a result of transfer of energy from the electrons to one or the other of the two radiation states by a scattering process, b. Quenching, which is an enforcement of the optical transition by collisions of the second kind, and, c. Polarization (γ_p) when the upper state is degenerate, or nearly so. Polarization may be caused by the induction of a temporary dipole moment or by reorientation of a dipole moment already present due to a neighboring ion. Kivel[23] extends the work of KBM to include line shift and applies the result to the He I spectrum. Kivel treats the interaction between electron and atom as a perturbation and expands the Schrodinger wave function with plane wave factors for the free electron (Born approximation). After correcting an algebraic error in Kivel's paper, as pointed out by Seay[9], Kivel's relations are expressed as follows:

(a) The contribution to the line width due to electrons is:

$$\omega_{1/2} = \left(\frac{2 n_e v \sigma}{3}\right) \sum_{l=l,\, l+1} \left(\frac{r_{n,l}}{a}\right)^2 2 \left| N \right| \left| \frac{4\epsilon}{E_{n,l} - E_{n,l-1}} \right| \quad (4\text{-}9)$$

where

$$\left(\frac{r_{n,l}}{a}\right)^2 \equiv \left(\frac{r_{n,l,0}}{a}\right)^{n,l-1,0}{}^2 = \frac{9}{4} n^2 (n^2 - l^2)$$

[22] Kivel, Bloom, and Margenau, Phys. Rev. 98, 495 (1955)
[23] B. Kivel, Phys, Rev. 98, 1055 (1955)

v = electron velocity

$\sigma = \pi \left(\frac{\hbar}{mv}\right)^2$

r_{nl} = matrix element for constant h

a = first Bohr orbit

ϵ = free electron energy

E_{nl} = term values

n = principle quantum number

(b) The contribution to the shift due to the electrons is:

$$\delta_i = 4.55 \cdot 10^{-8} n_e \left(\frac{e^2}{2akT}\right)^{1/2} \sum_{E_n > E_i} n \left(\frac{r_{ni}}{a}\right)^2 \exp -\left(\frac{\hbar \omega_{ni}}{kT}\right) - \sum_{E_n < E_i} n \left(\frac{r_{ni}}{a}\right)^2 \qquad (4\text{-}10)$$

where the matrix elements r_{nl} do not now have the simple form shown above for constant n.

$$\left(\frac{r_{n,l}^{n',l+1}}{a}\right)^2 = \frac{l+1}{2l+1} \left(R_{n,l}^{n',l+1}\right)^2 \qquad (4\text{-}11)$$

$$\left(\frac{r_{n,l}^{n',l-1}}{a}\right)^2 = \frac{l}{2l+1} \left(R_{n,l}^{n',l-1}\right)^2 \qquad (4\text{-}12)$$

The radial integrations R_{nl}^2 are tabulated by Bethe[7] up to n = 4. The first summation represents upward coupling excited by the electrons. A Boltzman velocity distribution for the electrons is assumed. The second sum represents downward coupling triggered by the electrons.

Note that for line broadening only the upper level is concerned; the broadening of the ground or lower metastable state being negligible. For the electron induced line shift, however, both levels must be considered. The broadening theory does not correct for the shielding of

the distant electrons (plasma cut-off) and thus gives values for broadening which are too large. Note also that the line shift theory uses the Born approximation for even the zero energy electrons and requires the shift to be small compared with level separations. The latter requirement is rather restrictive for the $4d\,^3D$ level, where the 4d-4f separation is only 7.78 cm^{-1}.

EXPERIMENTAL OBSERVATIONS OF LINE BROADENING

Dickerman[24] describes a technique for applying the Holtzmark theory to the broadening of the H_β line. He applies the Holtzmark theory to each component, compounds the components to obtain a theoretical profile, then fits observations to this profile, with n_e and T being defined through the Saha equation. Seay[9] includes the electron effects in the Holtzmark theory for He as follows:

"(1) The splitting of the line due quadratic Stark effect was calculated as a function of the electronic field due to ions.

(2) An electron - broadened line shape was assigned to each Stark component.

(3) Each component was integrated over an ion probability (Holtzmark) distribution function.

(4) The components were added graphically to give a total line shape.

(5) The total line shape was shifted by an amount depending on the electron density and temperature (Kivel's electron impact theory)."

While each of the above methods is essentially correct and each has its merits, both methods involve the computation of line profiles. Without the use of high speed data processing equipment this approach was considered too cumbersome for the present application. Instead the simple approach coutlined below was attempted (with a mind toward automation) for temperature determination.

The simplest and most applicable formulation of each theory was selected. These relations involving half-widths and shift as functions

[24] P. J. Dickerman, J. App. Phys. 29, 598, (1958)

of temperature and ion density were then plotted with ion density on a log scale and temperature a linear scale. Plots were made for various values of width or shift for each line. Separate sheets were used for each relation. (See Figs. 8 through 15) All plots were made on the same scale. Also plotted to the same scale was the Saha equation:

$$\frac{\alpha^2}{1-\alpha^2}\,\frac{p}{kT} = \frac{(2\pi m)^{3/2}(kT)^{3/2} Pf_e\, Pf_{He^+}\, e^{-T_{ion}/T}}{h^3\, Pf_{He}} \qquad (4\text{-}13)$$

where $\alpha = n_e/n_e + n_o$

p = pressure

m = reduced mass

T = temperature

$Pf_e = 2$ = partition function for the electrons.

$Pf_{He^+} = 2$ = partition function for the He ions.

$Pf_{He} = 1$ = partition function for the He atoms.

n_o = neutral particle density

n_e = electron (ion) particle density.

(See Figs. 18 and 19)

The theoretical plots were then entered with measured line width and the Saha equation with measured pressure and the two plots superimposed to obtain a simultaneous solution. The experimental data and results were tabulated. (See Table I.) Figs. 20 through 22 are microdensitometer tracing samples of the raw data. Fig. 20 is an example

Experimental Data						Theoretical Results			
Wavelength A	Run	Half-width $\cdot 10^{12}$ (sec^{-1})	Shift $\cdot 10^{12}$ (sec^{-1})	Press. (Atmos.)	Power (kw)	T_1 (ev)	n_{e_1} $\cdot 10^{15}$ (cm^{-3})	T_2 (ev)	n_{e_1} $\cdot 10^{15}$ (cm^{-3})
3889	18E	.88 ±.03		1.19	23.8	1.01	0.49		
	19G	3.5 ±0.2		3.38	35.5	1.09	1.95		
	10C	3.7 ±0.2		2.09	28.0	1.12	2.1		
	10A	3.9 ±0.3	0.60 ±0.03	2.02	28.0	1.13	2.3	1.75	105
	20C	6.3 ±1.4	0.47 ±0.11	1.14	78	1.21	3.7	1.8	84
4026	18E	20.0 ±3.0		1.19	23.8	1.05	0.74		
	18M	29 ±2		1.24	20.6	1.09	1.2		
4471	10A	27 ±4	4.7	2.02	28.0	1.17	3.4		
	6F	62 ±10	13	1.68	15.2	1.27	7.6		
4713	18E		0 ±0.5	1.19	23.8				

T_1, n_{e_1} = Values determined from Kivel's electron broadening formula.

T_2, n_{e_2} = Values determined from Kivel's electron shift formula.

TABLE I

of the strong, narrow 3889 helium line superimposed on a high contamination (mostly iron) background. Fig. 21 shows the same line with a much lower contamination level. Fig. 22 shows the very broad 4026 helium line with virtually no contamination. These figures also show why the Holtzmark theory was not used. Holtzmark theory is successful because it accurately (as per theorem a, sect. 4.c.(1). above) predicts line contours far from the line center. We rejected this theory because the line contours far from the line center were often masked completely by impurities.

5. DISCUSSION

A. Molecular Spectra

Of the temperature measurement techniques considered, the intensity variation in band spectra provide the most accurate, consistent, and reliable measurements of temperature. Because of the high degree of accuracy to which the molecular constants are known the theory itself contains very little systematic error. The primary source of error lies in the ± 1 uncertainty in determination of the intersection quantum number. This results in an error of $\pm$ 400 ^{o}K. The contributing factors to this error are the emulsion density gradient, the existence of fine structure perturbation, and contamination by strong spectral lines of foreign elements. The principle limitation lies in the narrow range of sensitivity. For temperatures in excess of 6000 ^{o}K dissociation begins to occur and, in addition, at this temperature the intersection is masked by the following band head. Below 3500 ^{o}K the intersection falls too close to the vertex of the Fortrat parabola to allow a branch envelope to be drawn. Also, at lower temperatures the band excitation (intensity) is reduced. Since the technique requires only a small amount of nitrogen (and carbon, furnished by the electrodes) which is found as an impurity in most industrial bottled gas, or which may be easily introduced (by allowing an air leak), it portends to a wide application.

B. Stark Broadening.

The Stark broadening method of temperature measurement is considered usatisfactory in this application. The experimental difficulties of determining the line contour, or even a shape parameter such as the half width, have been described above. In the application of the theory several difficulties exist. For the line widths and ion

densities encountered in this experiment, neither inequality 4-5 nor 4-6 hold. Since the half width is neither far from, nor close to, the line center, theorem (b), sect. 4.c.(1), is of little help. The above are offered as explanations as to why the Lindholm theory for ion induced broadening and shift do not produce intersection with the Saha equation. The electron broadening and shift theory probably has only a slight advantage over Lindholm's theory in this application. A glance at the Saha equation (Figs. 18 and 19) will reveal however that almost any crude determination of ion density will yeild a temperature in the range 1.0 - 1.5 electron volts. The limitations, then, which preclude the use of Stark broadening for temperature determination in this application are:

a. The formulations are extremely complex and involve many inaccurately known parameters. These formulations must be applied to so many of the components of broadening as to make the amount of work involved prohibitive.

b. The theory is inconclusive as to the proper method of including electron effects.

c. The broadening mechanism is so powerful that the total intensity of the line is spread over a wide wavelength region (5-20 A). This requires long exposures and/or high plate sensitivity with attendant experimental difficulties.

d. The presence of contaminants may mask a broaden line completely or at least destroy its measured intensity distribution.

e. The reduction method requires the determination of two parameters (n_e and T) with the problem of simultaneous solutions of transcental equations.

C. Geometrical Considerations

We have shown above (although not conclusively for the higher values) that two different temperatures have been measured for the arc. The reason for this is simple. Maecker[25] shows an isothermal field plot of temperatures in a carbon arc with a 200 amp current and a 4.5 cm gap length. A temperature of about 10,000 ^{o}K is indicated in the center of the arc falling to about 500 ^{o}K at a radial distance of one gap length from the center. Photographs taken of the USNPGS arc jet compare very favorable with those taken by Maecker for intensity distribution. Assuming the same type of temperature distribution, the following plausability argument is given for the temperatures measured. Near the center of the arc where the temperature and ion density are high the excitation and intensity of the atomic helium radiation is a maximum. Thus the line broadening technique will yield a central, or core, temperature. Molecular dissociation of the CN molecules occurs as the molecules near the hot core and therefore no molecular radiation originates in the core. Near the outer edge of the arc, where the molecules exist, the temperature is lower and the molecular radiation is much more intense than atomic radiation. Thus the band intensity technique measures this outer temperature.

It is noteworthy that in contrast to Maecker's water stabilized arcs, the arc considered here was stabilized only by the small radial pressure gradient induced by the gas swirl. As indicated by the movies, the arc showed a marked tendency towards rotational instability. This

[25]Finkelnburg and Maecker, Electrische Bogen und Thermisches Plasma, Handbuch der Physik, Band XXI, Gas Discharges II, S. Flugg (Ed.), Springer-Verlag, Berlin, Gottingen, Heidelberg, 1956.

precluded any attempt to study small regions of the arc where the temperature might be nearly constant. It should be noted that there was one configuration which showed a stable tendancy. At very low power levels (.05-.2Kw) and for low pressures (3-5 psig) the arc was observed to strike to the edge of the hollow anode and spiral into the axis. The anode end of the arc was then essentially "swallowed" by the anode nozzle and the arc tended to stabilize on the nozzle axis. This condition was difficult to duplicate, however.

One spectrogram of the plasma jet was taken of the region just downstream (outside) of the nozzle. In this configuration the expanding portion of the deLavel nozzle was removed and only the drilled carbon anode was used. The working fluid was helium and yet this spectrogram showed no atomic helium lines. The CN band spectra were very strong and temperature measurements obtained were comparable with the other band spectra measurements. A reduction in temperature with increasing distance from the nozzle was also observed.

6. CONCLUSIONS

The arc jet used as wind tunnel.

a. For stagnation temperatures of more than 5000°K and flows of ionized gases with relative ionization of greater than one percent, more than 100 volts of DC power supply must be used to combat anode and cathode potential drops and couple the necessary energy into the gas.

b. The carbon anode design must be considered carefully to prevent spalling and cracking and to provide efficient nozzling. The external nozzle must provide for uniform super sonic flow in a test section. The test section must be of such design to accomodate a window.

c. To be meaningful temperature measurements must be made in the test section where conditions are uniform and well defined.

d. For ion flows and magnetohydrodynamic studies, high powers (above 100 kw) and short nozzles must be used to combat recombination. A magnetic nozzle would find useful application here.

The arc jet used as a plasma generator.

The configuration of the arc jet at USNPGS is unsuited for use as a plasma generator because:

a. The highly ionized region is confined to a narrow core between the electrodes. This core has variable properties and is not configurationally stable.

b. The arc characteristics are not reproducable due to the above instabilities.

The Spectrographic measurements of the arc jet may be briefly summarized as follows:

a. Temperatures obtained using the molecular spectra were in the

range of 5000-5300°K. These are not the temperature of the ionized core but they do define a temperature sheath surrounding the hot inner core.

b. The electron line broadening of atomic spectra gave temperatures in the neighborhood of 1.12 ev (13,000°K). Below 1.6 ev (18,550 K) the temperature is relatively insensitive to large changes in density.

c. The line broadening theory used was unsatisfactory for simple temperature determinations.

FIG. 1

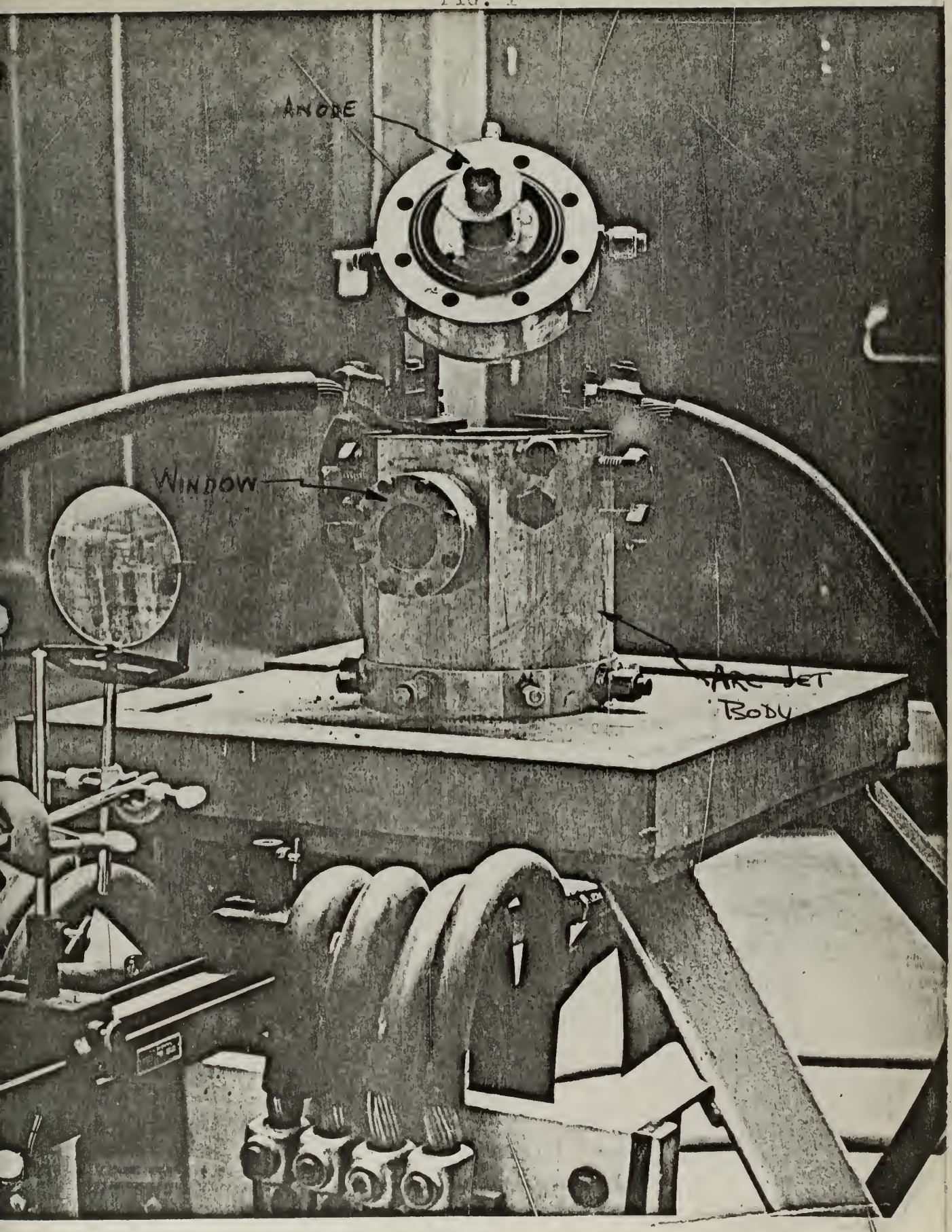

Fig. 1

Fig. 2

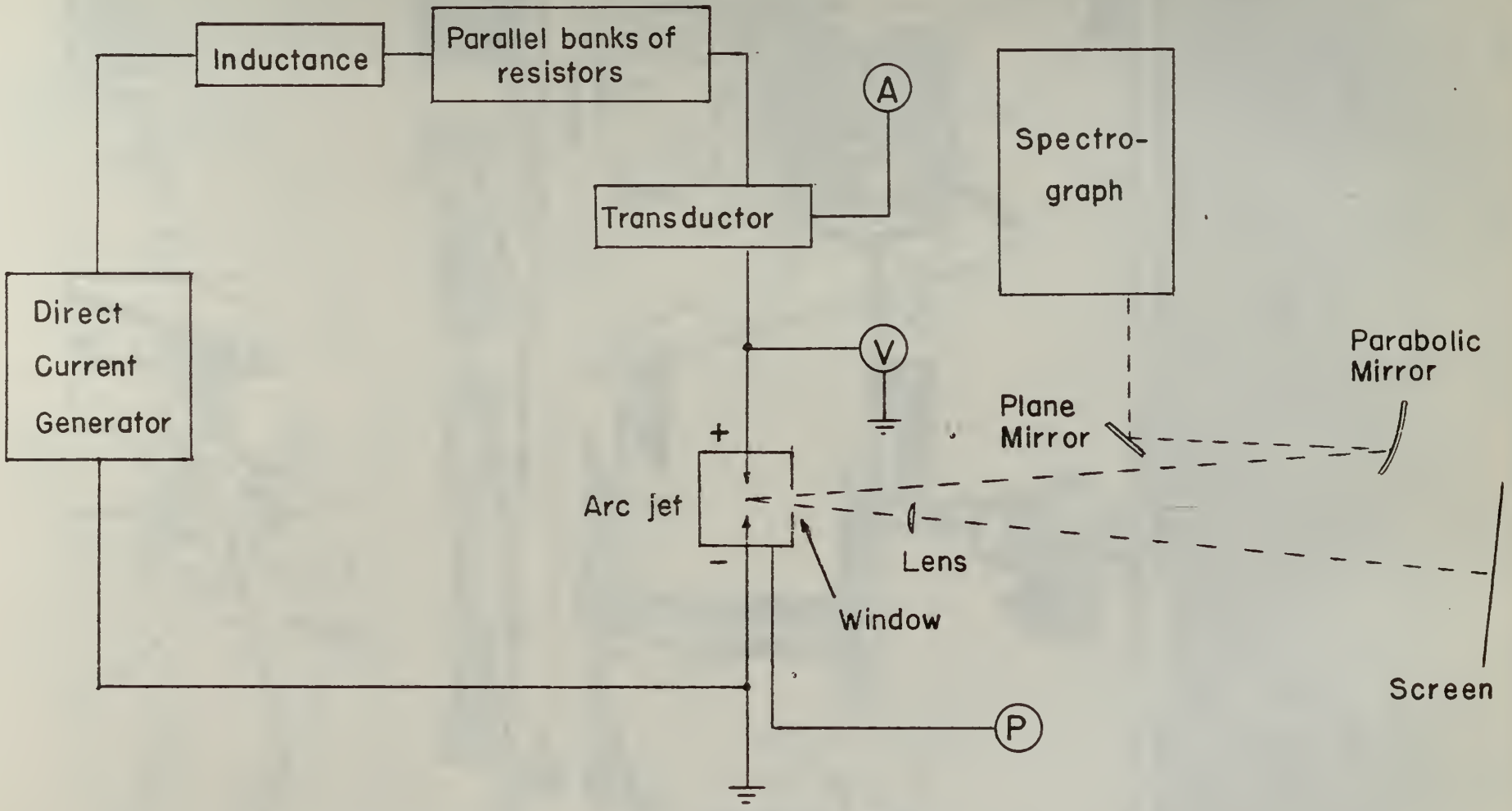

Schematic of the Experimental Setup

Fig. 3

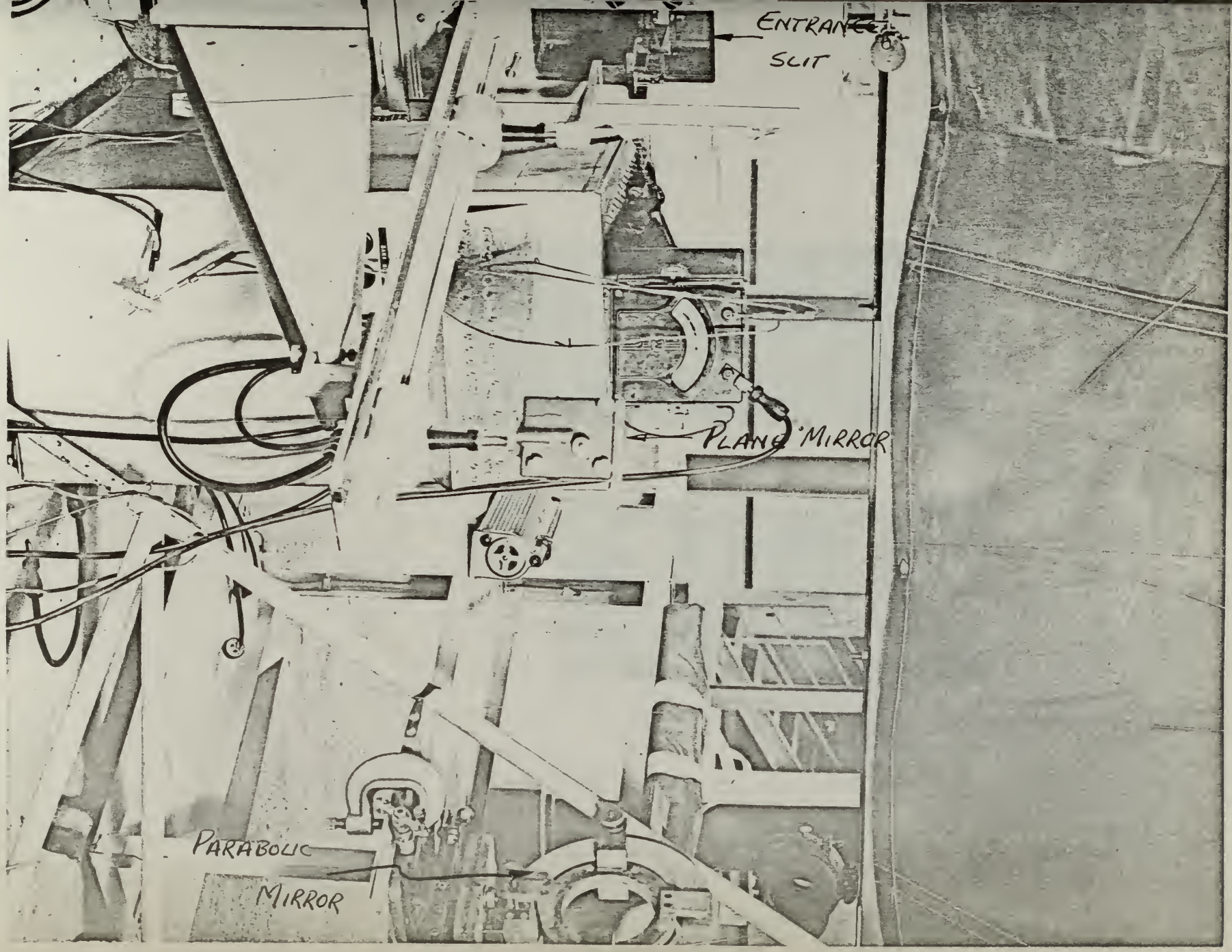
ENTRANCE
SLIT
PLANE MIRROR
PARABOLIC
MIRROR

SPECTROGRAM 0-1 CN BAND

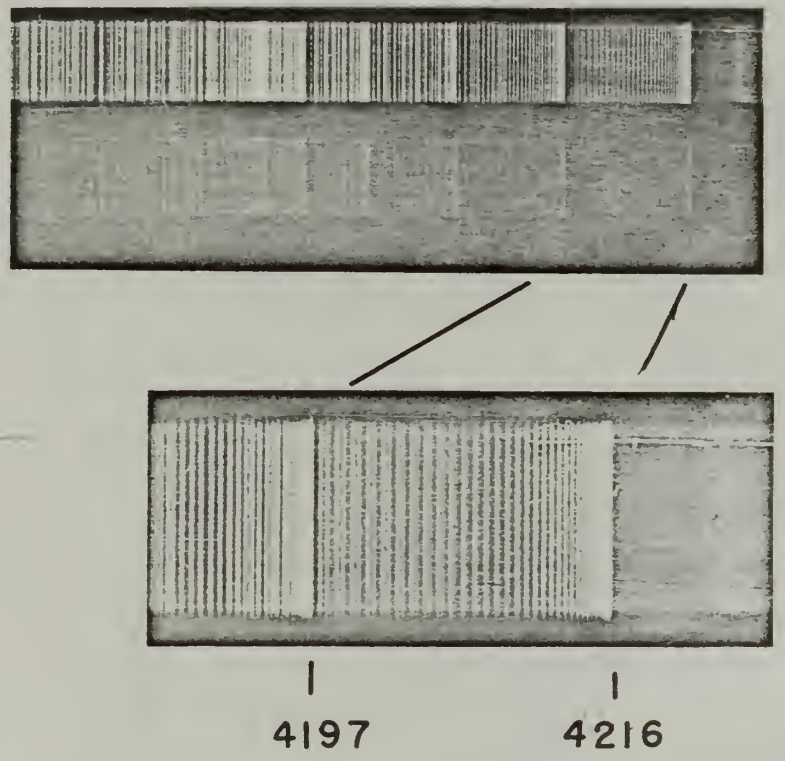

Fig. 4

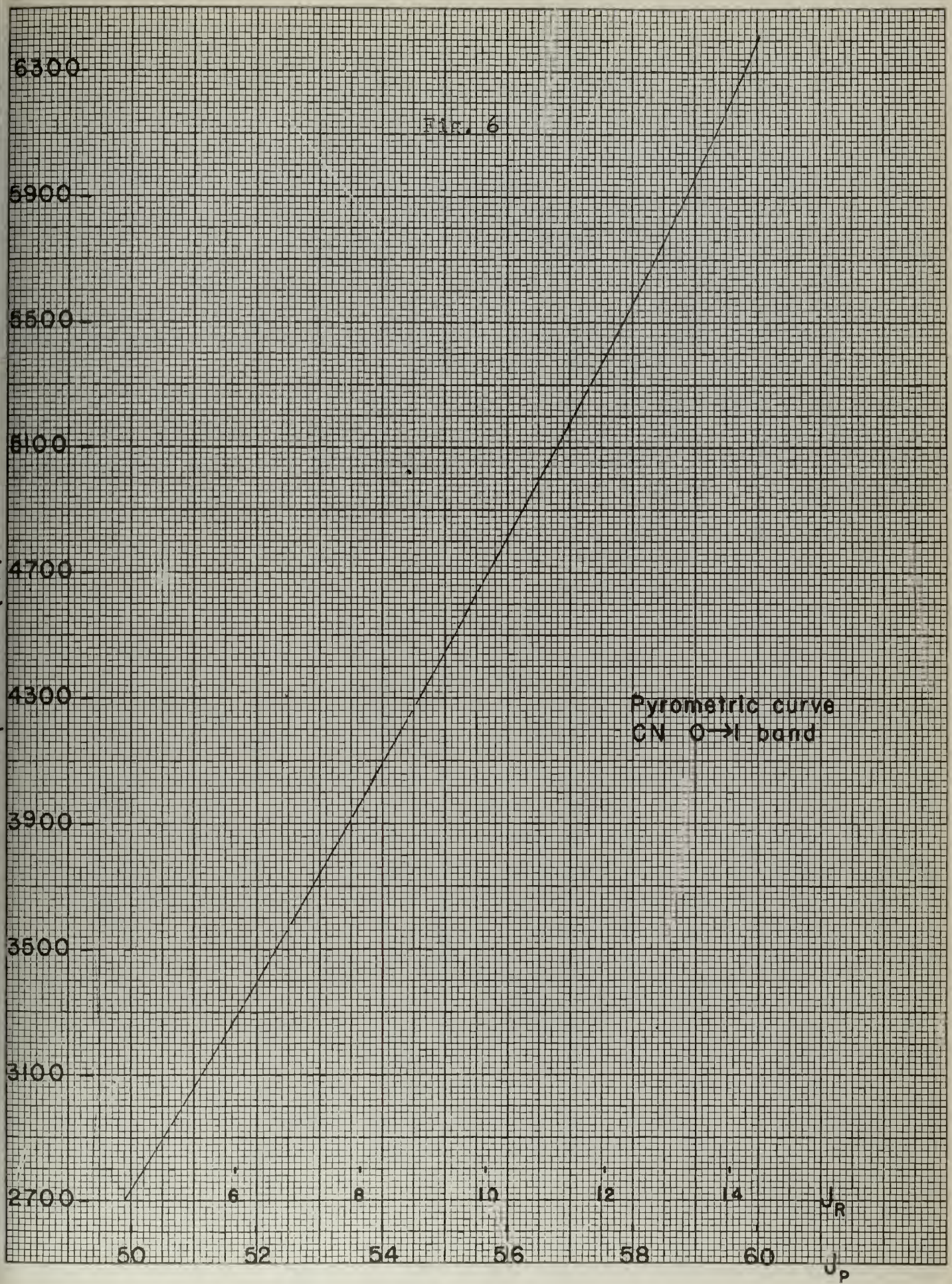
Fig. 6
6300
5900
5500
5100
4700
4300
3900
3500
3100
2700
Pyrometric curve
CN 0→1 band
50
52
54
56
58
60
J_P
6
8
10
12
14
J_R

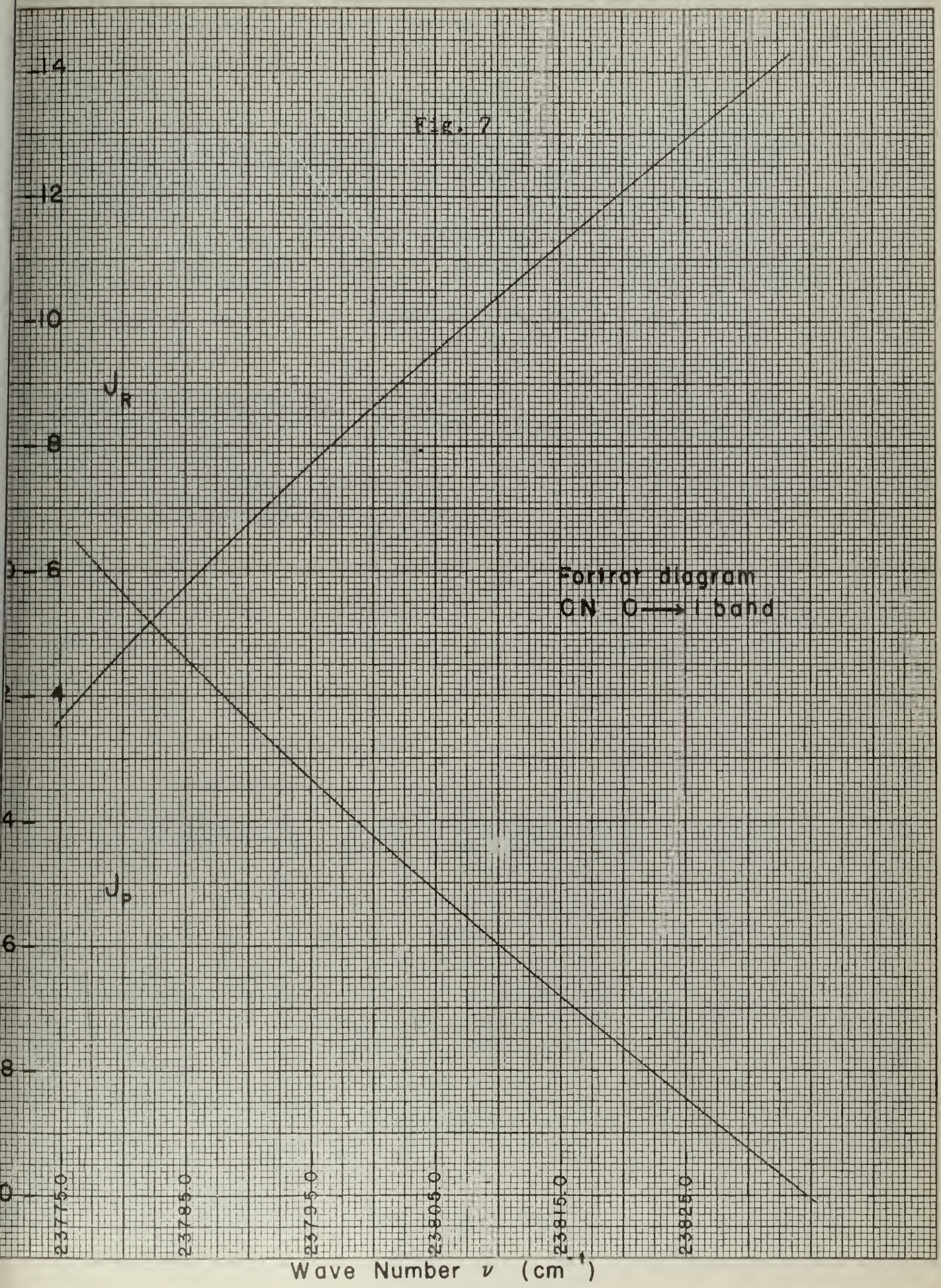
Fig. 7
14
12
10
8
6
4
2
0
J_R
J_P
Fortrat diagram
CN O⟶ i band
23775.0
23785.0
23795.0
23805.0
23815.0
23825.0
Wave Number ν (cm^{-1})

Fig. 8

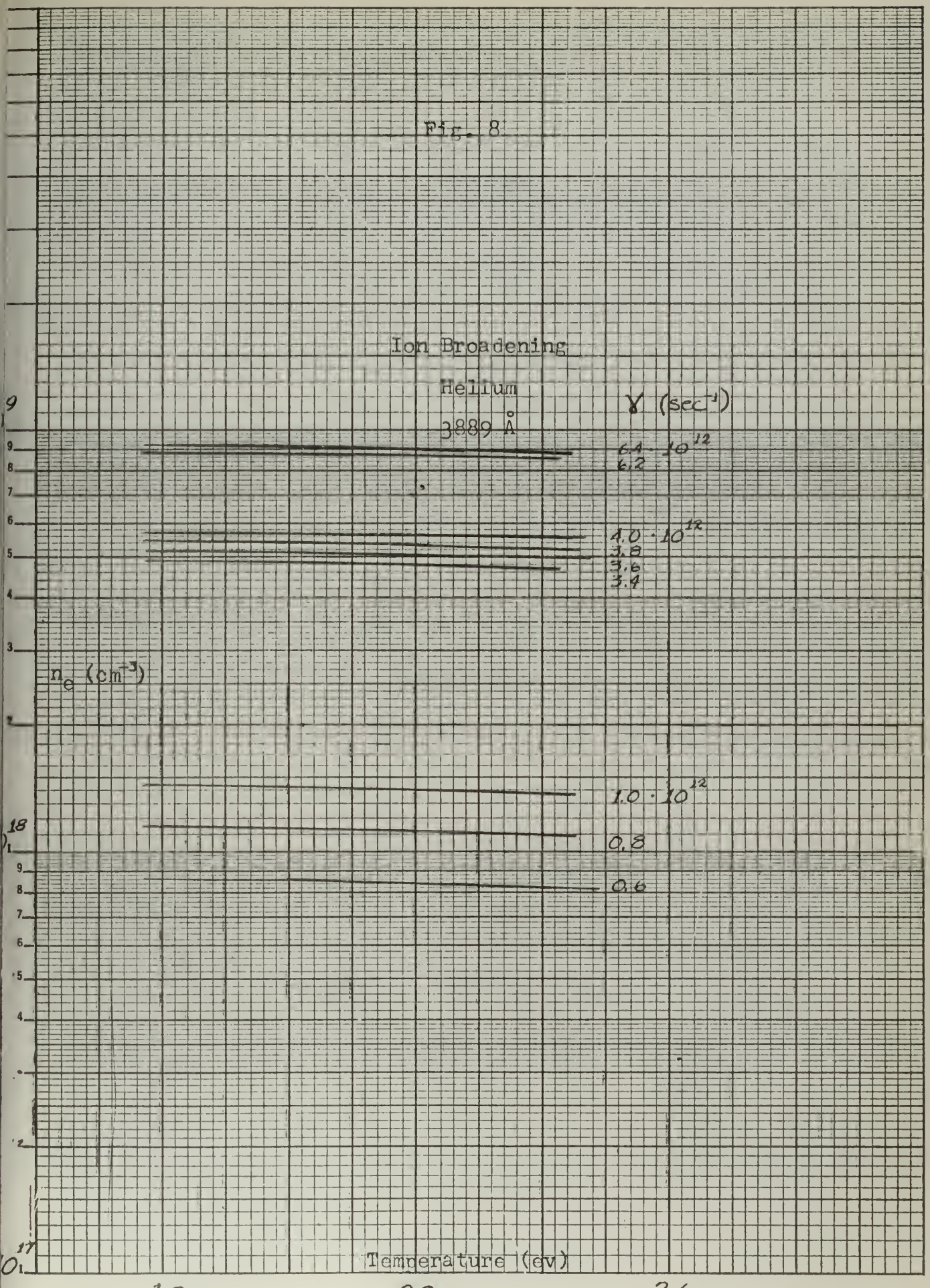
Ion Broadening
Helium
3889 Å
γ (sec⁻¹)
6.4 · 10¹²
6.2
4.0 · 10¹²
3.8
3.6
3.4
1.0 · 10¹²
0.8
0.6
n_e (cm⁻³)
Temperature (ev)
1.8
2.2
2.6

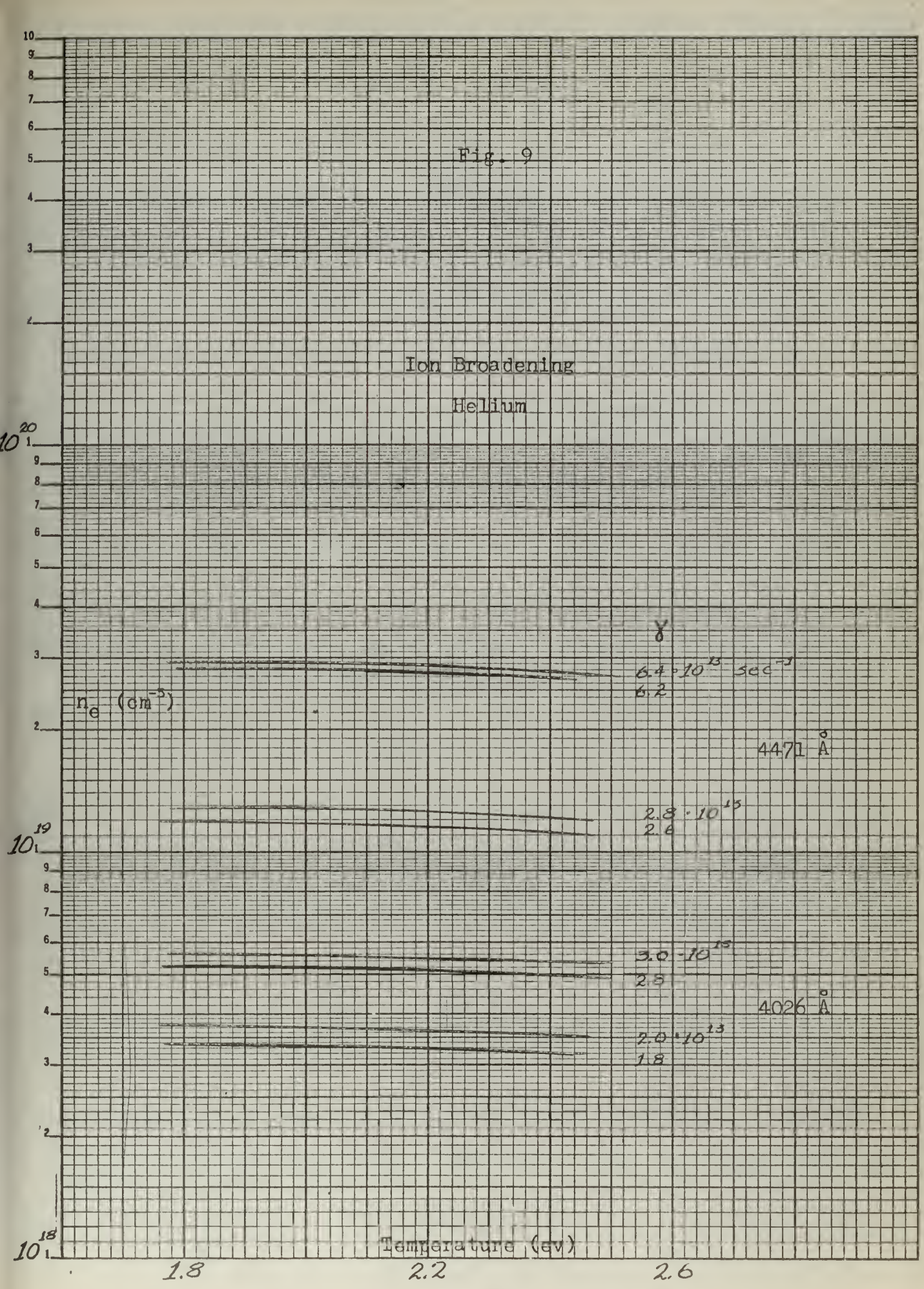
Fig. 9
Ion Broadening
Helium
γ
6.4 · 10^15 sec^-1
6.2
4471 Å
2.8 · 10^15
2.6
3.0 · 10^15
2.8
4026 Å
2.0 · 10^15
1.8
n_e (cm^-3)
10^20
10^19
10^18
Temperature (ev)
1.8
2.2
2.6

Fig. 10

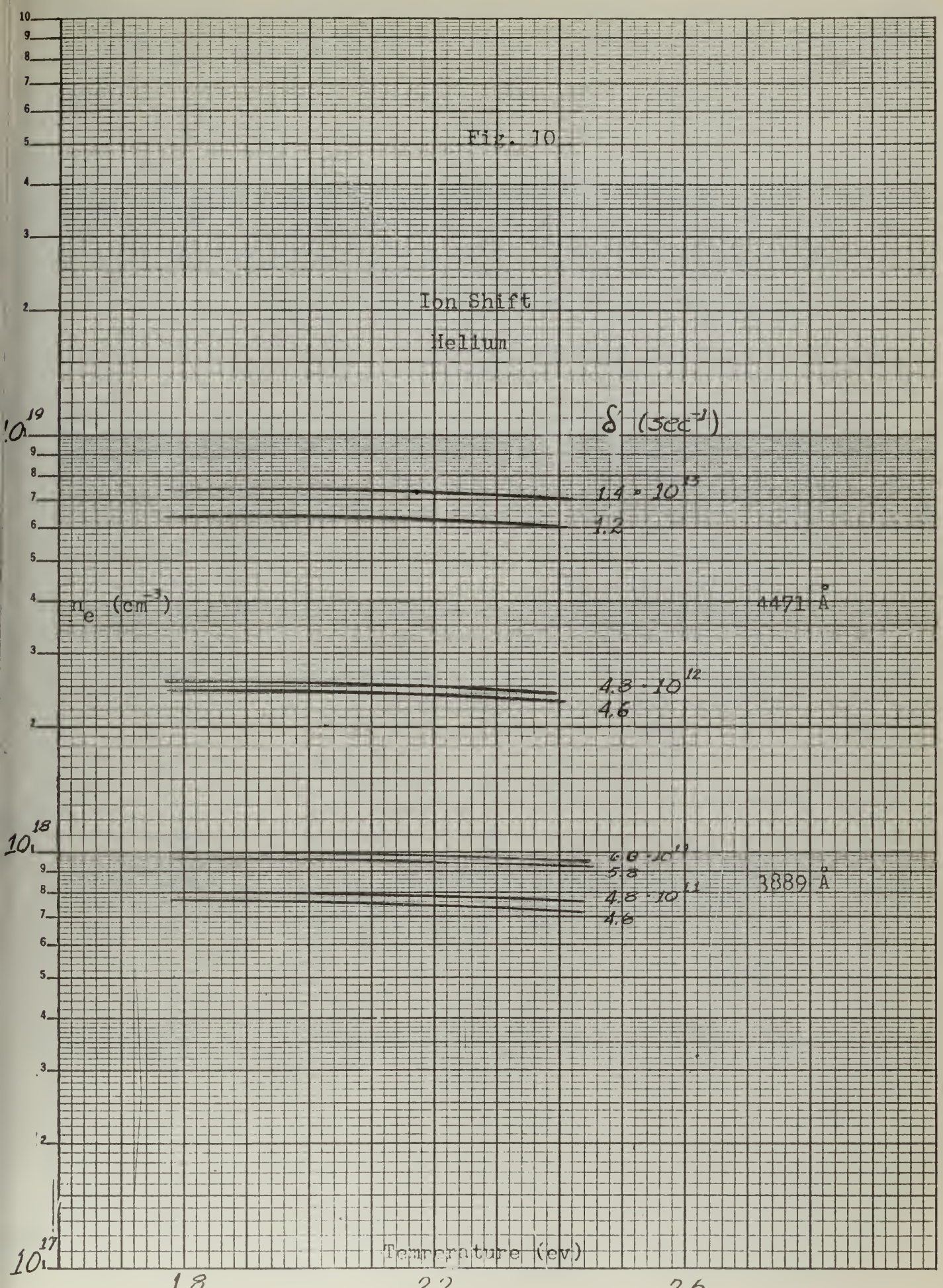
Ion Shift
Helium
δ (sec⁻¹)
1.4 × 10¹³
1.2
4471 Å
n_e (cm⁻³)
4.8 · 10¹²
4.6
10¹⁹
10¹⁸
10¹⁷
6.8 · 10¹¹
5.8
4.8 · 10¹¹
4.6
3889 Å
Temperature (ev)
1.8
2.2
2.6

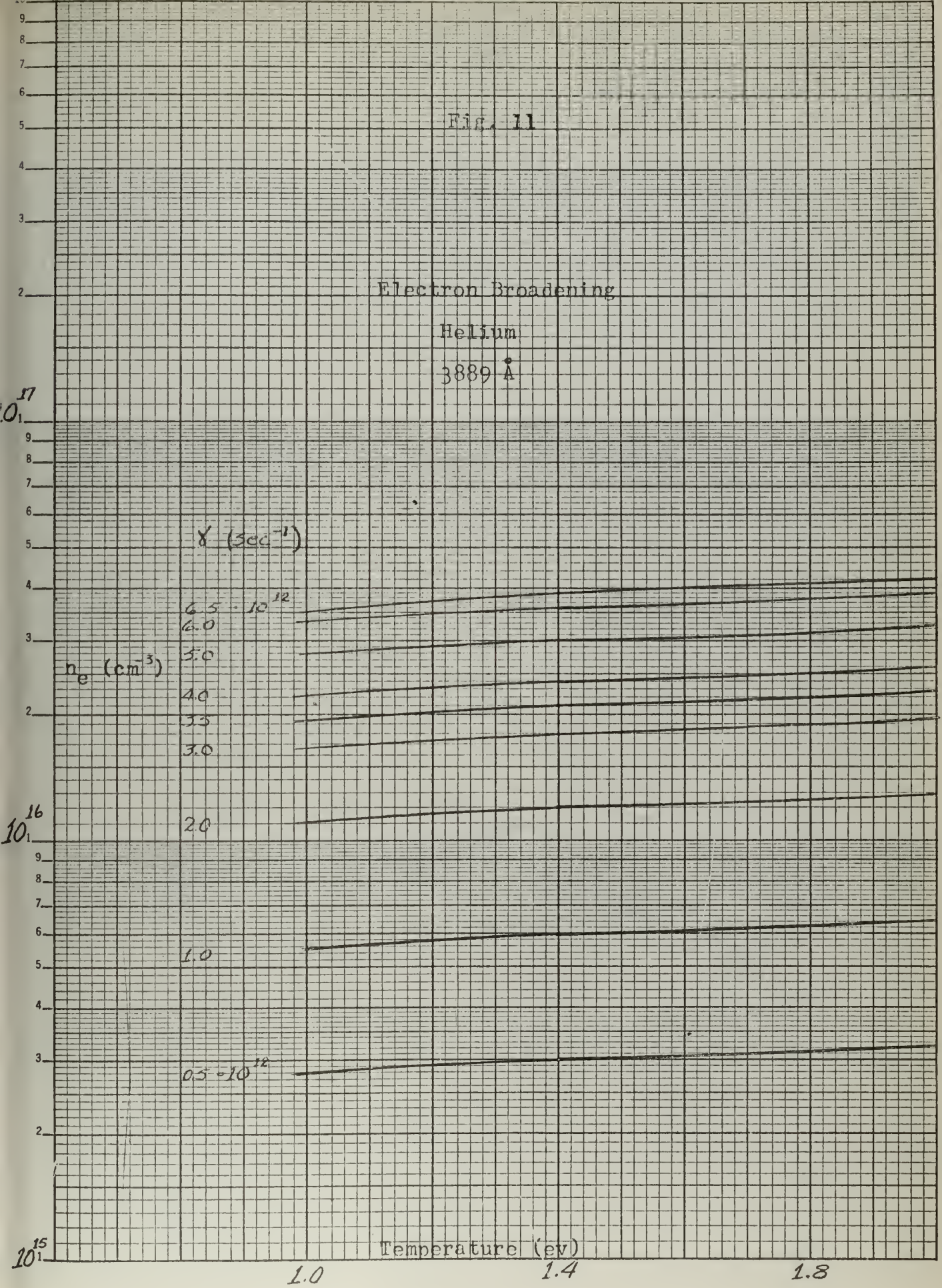
Fig. 11
Electron Broadening
Helium
3889 Å
γ (sec⁻¹)
6.5 · 10¹²
6.0
5.0
4.0
3.5
3.0
2.0
1.0
0.5 · 10¹²
n_e (cm⁻³)
10¹⁷
10¹⁶
10¹⁵
Temperature (ev)
1.0
1.4
1.8

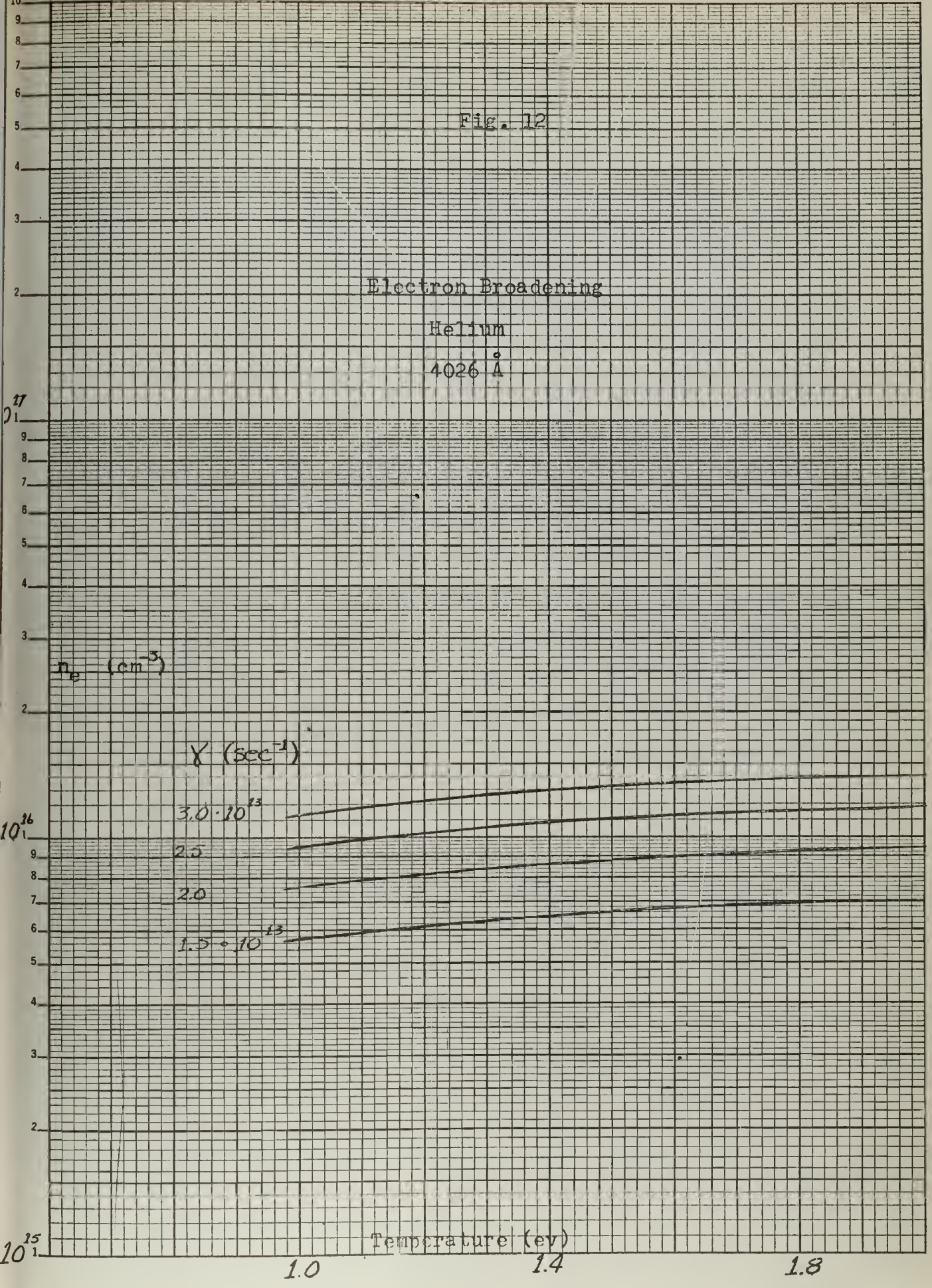
Fig. 12
Electron Broadening
Helium
4026 Å
n_e (cm^{-3})
χ (sec^{-1})
$3.0 \cdot 10^{13}$
2.5
2.0
$1.5 \cdot 10^{13}$
10^{17}
10^{16}
10^{15}
Temperature (ev)
1.0
1.4
1.8

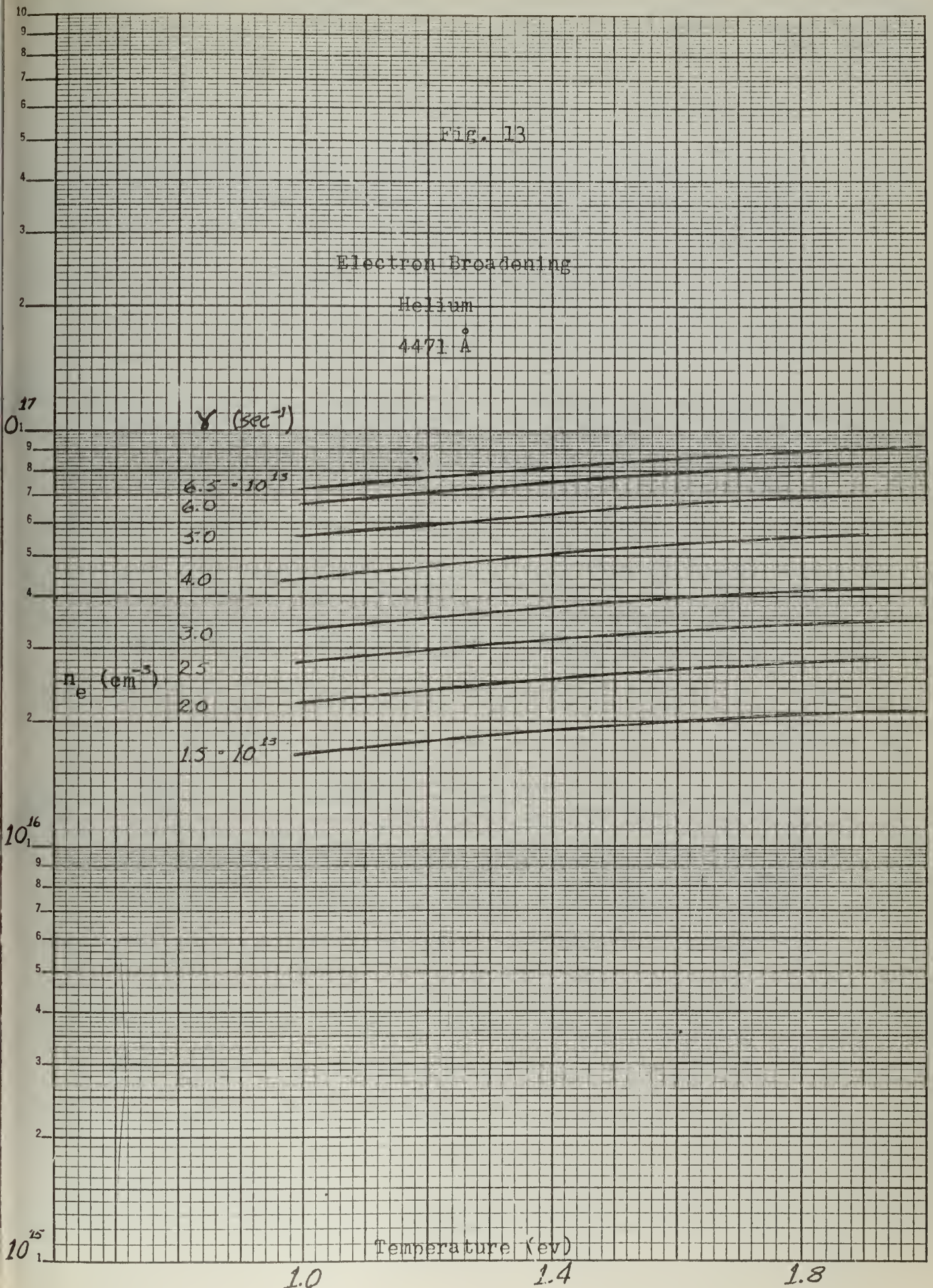
Fig. 13
Electron Broadening
Helium
4471 Å
γ (sec⁻¹)
6.5 · 10¹³
6.0
5.0
4.0
3.0
2.5
2.0
1.5 · 10¹³
n_e (cm⁻³)
10¹⁷
10¹⁶
10¹⁵
Temperature (ev)
1.0
1.4
1.8

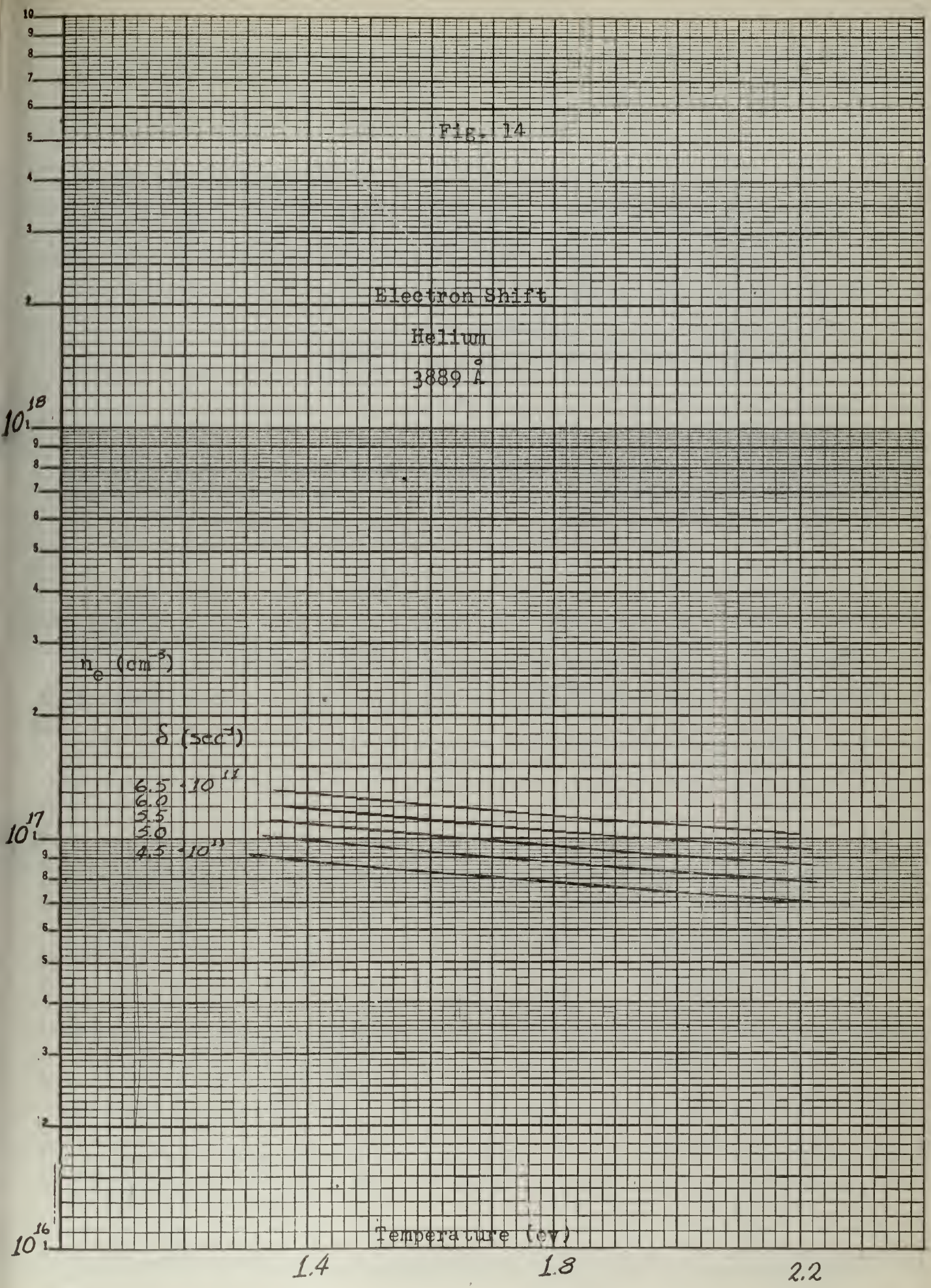
Fig. 14
Electron Shift
Helium
3889 Å
n_e (cm^{-3})
10^{18}
10^{17}
10^{16}
δ (sec^{-1})
6.5 ×10^{11}
6.0
5.5
5.0
4.5 ×10^{11}
Temperature (ev)
1.4
1.8
2.2

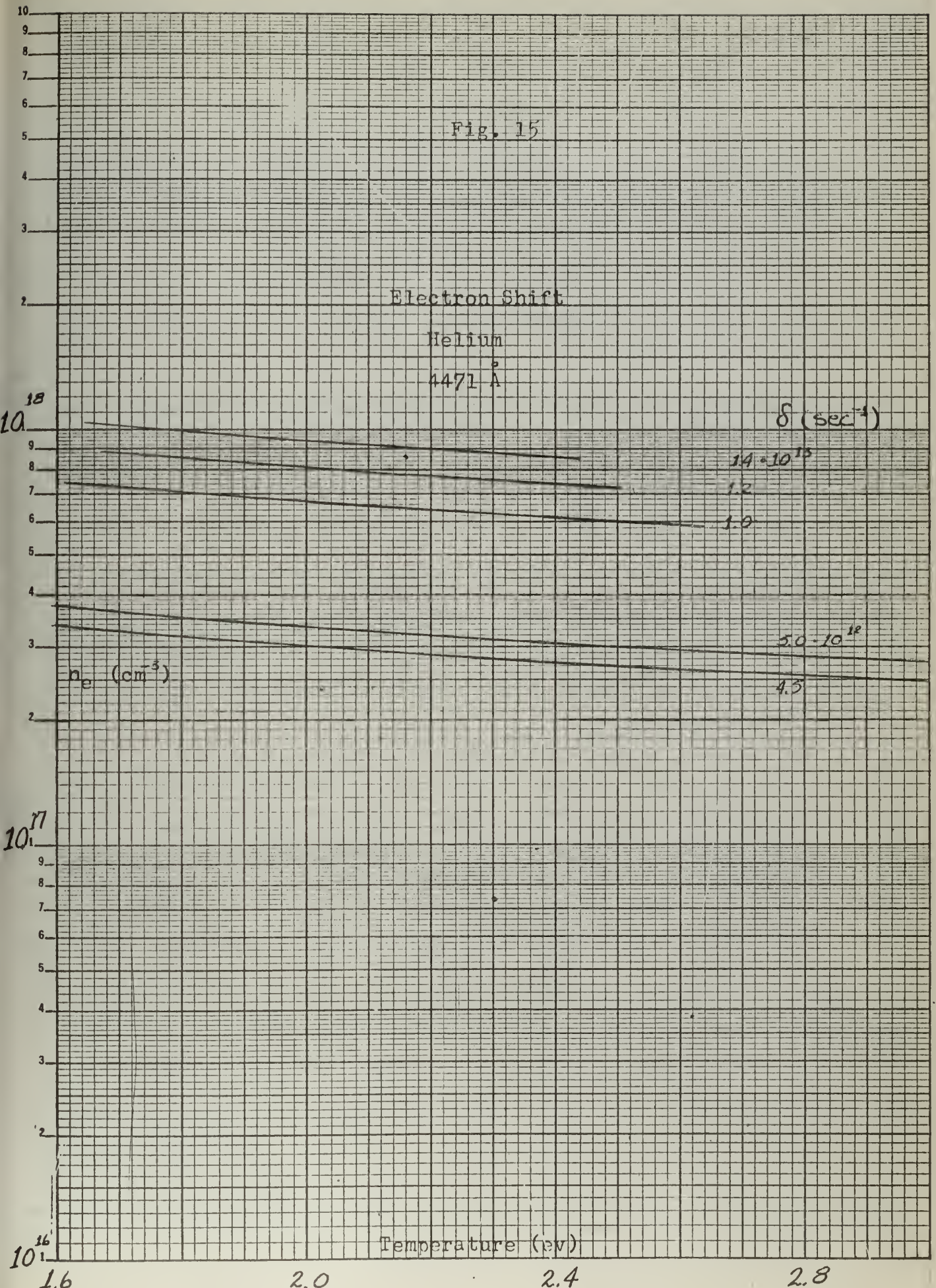
Fig. 15
Electron Shift
Helium
4471 Å
δ (sec⁻¹)
1.4 · 10¹⁵
1.2
1.0
5.0 · 10¹⁴
4.3
n_e (cm⁻³)
10¹⁸
10¹⁷
10¹⁶
Temperature (ev)
1.6
2.0
2.4
2.8

Fig. 16

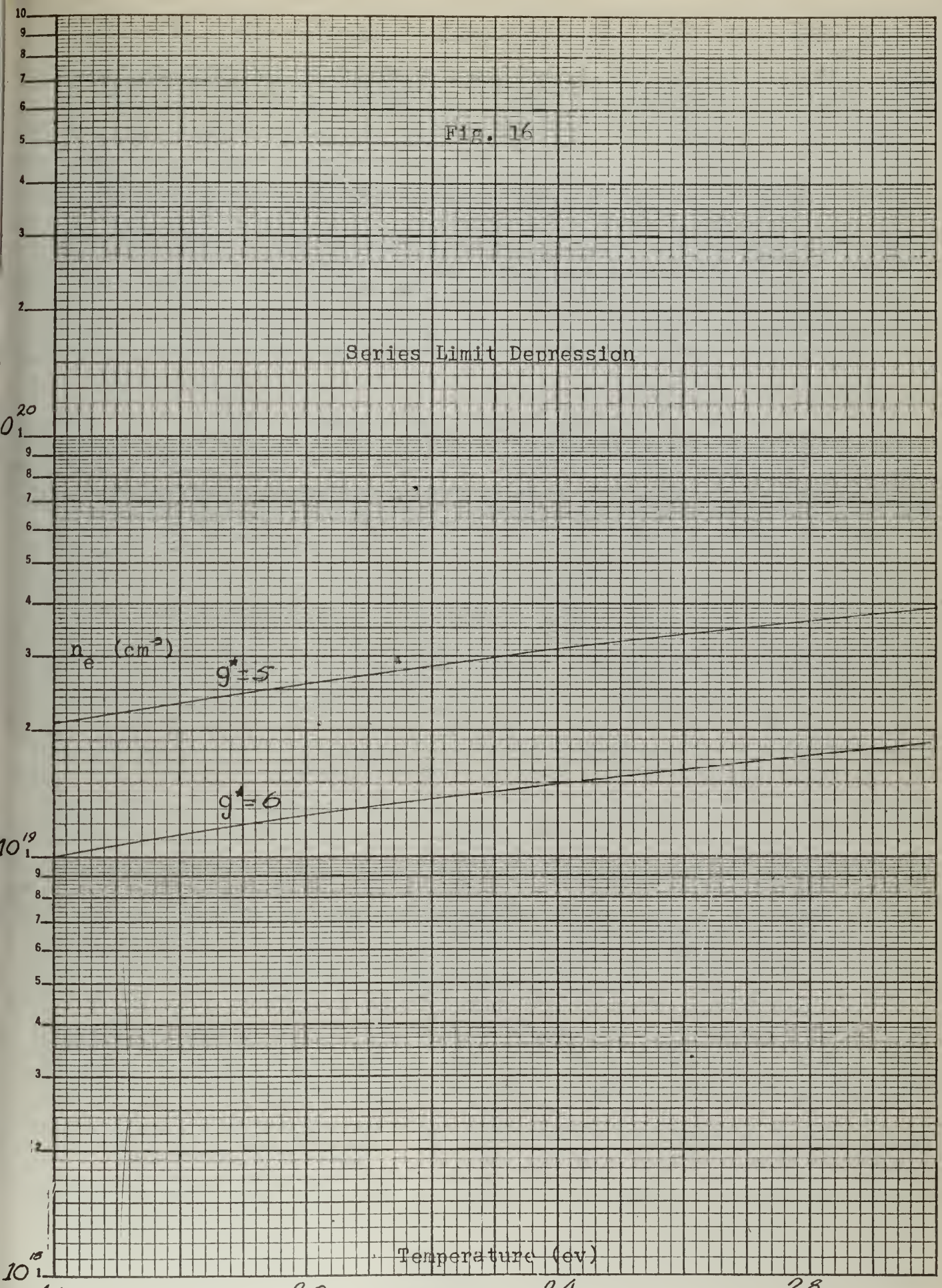
Series Limit Depression
n_e (cm^{-3})
$g^* = 5$
$g^* = 6$
10^{20}
10^{19}
10^{18}
Temperature (ev)
1.6
2.0
2.4
2.8

Fig. 17

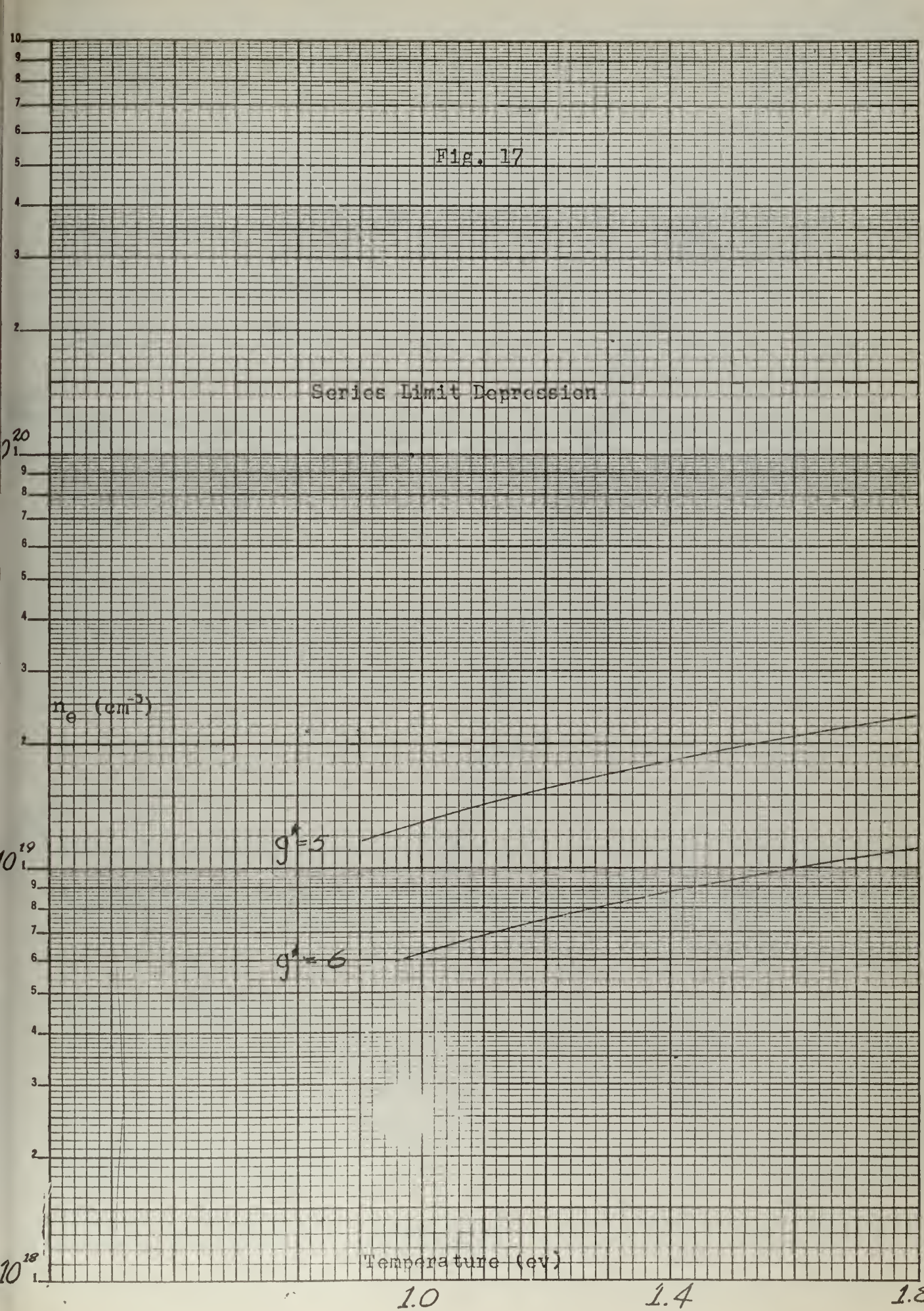
Series Limit Depression
n_e (cm^{-3})
10^{20}
10^{19}
10^{18}
$g^* = 5$
$g^* = 6$
Temperature (ev)
1.0
1.4
1.8

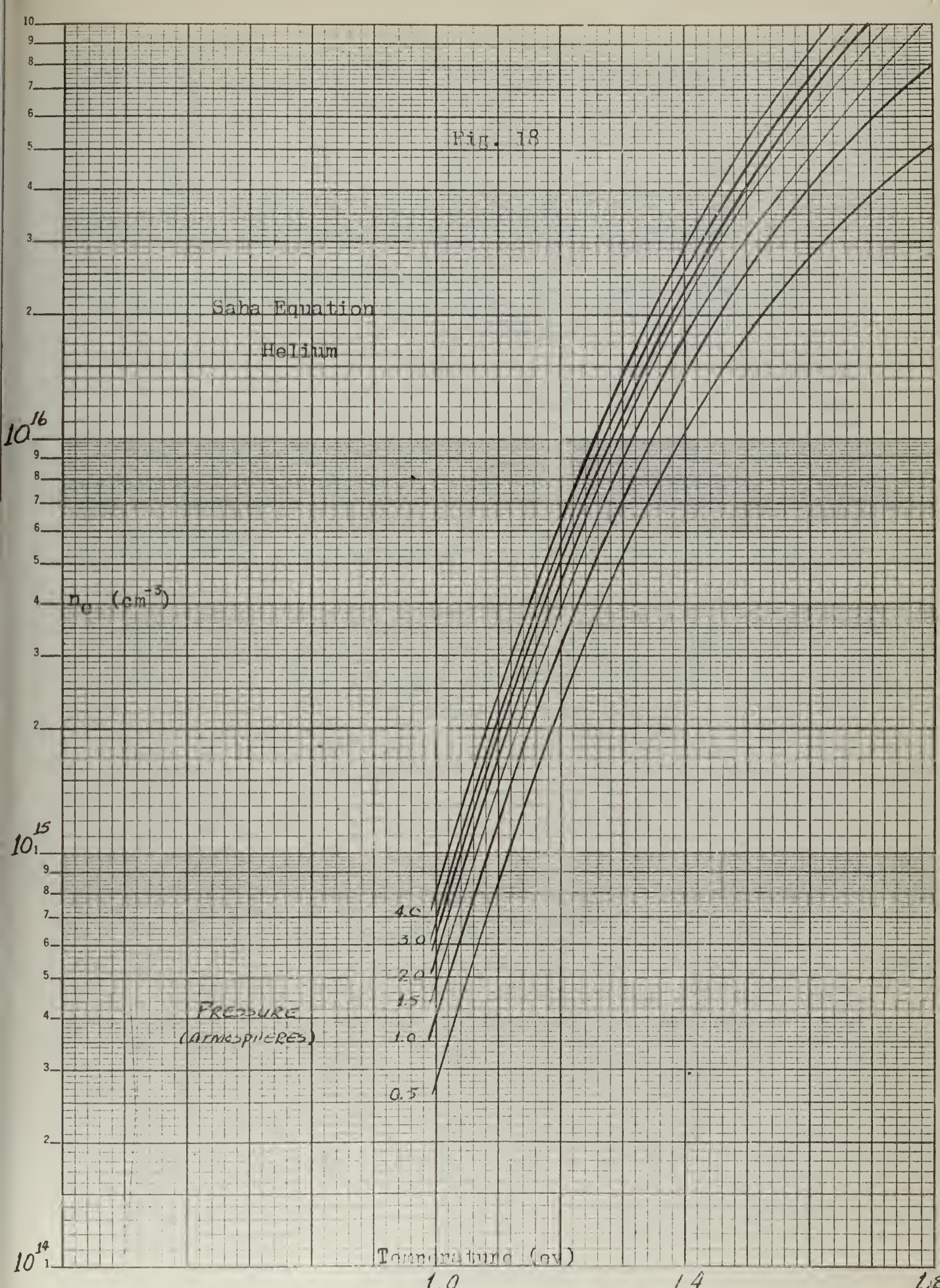
Fig. 18
Saha Equation
Helium
10^{16}
n_e (cm^{-3})
10^{15}
10^{14}
4.0
3.0
2.0
1.5
1.0
0.5
Pressure
(Atmospheres)
Temperature (ev)
1.0
1.4
1.8

Fig. 19

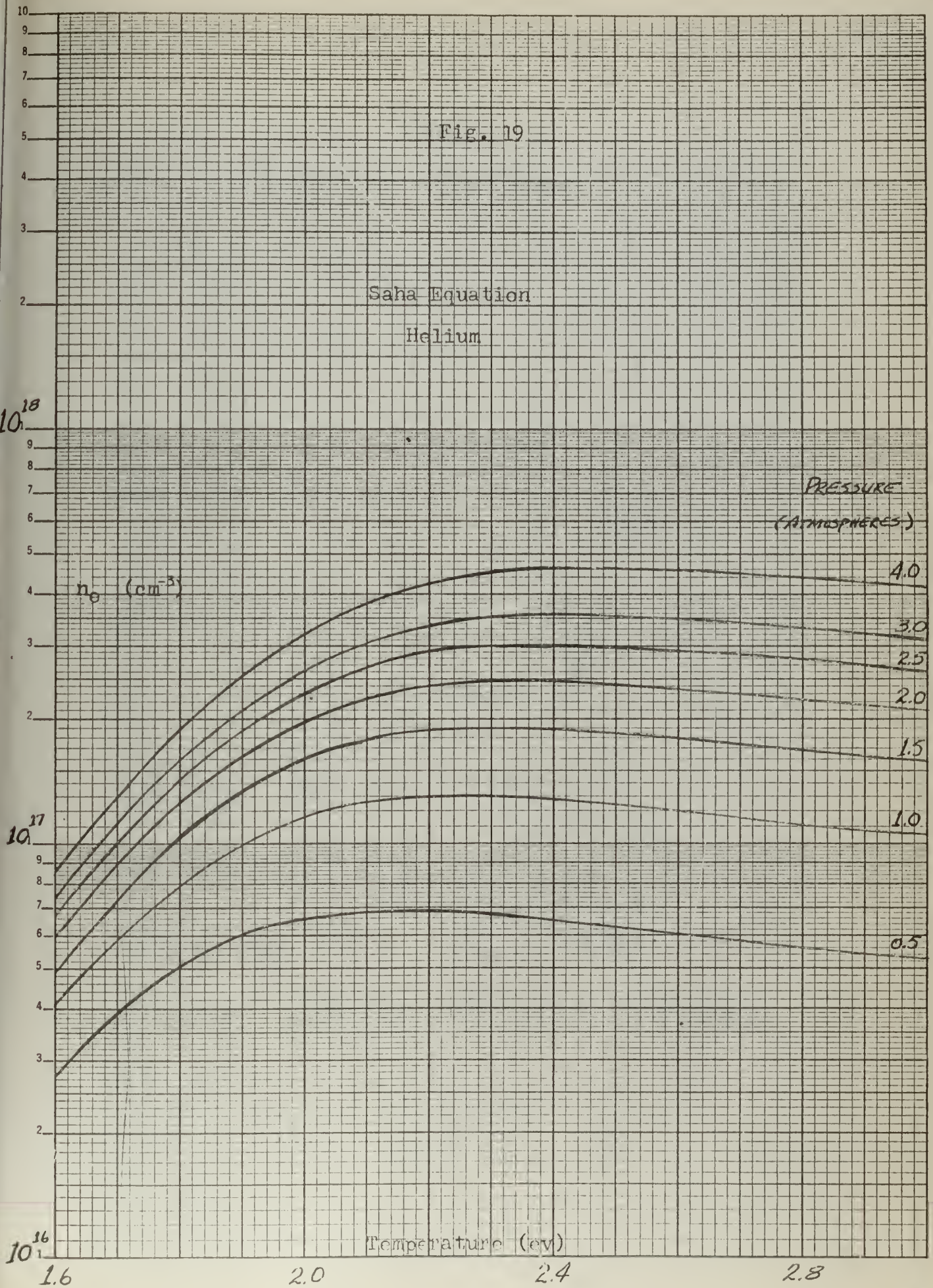
Saha Equation
Helium
10^{18}
10^{17}
10^{16}
n_e (cm^{-3})
Pressure
(Atmospheres)
4.0
3.0
2.5
2.0
1.5
1.0
0.5
Temperature (ev)
1.6
2.0
2.4
2.8

Fig. 20

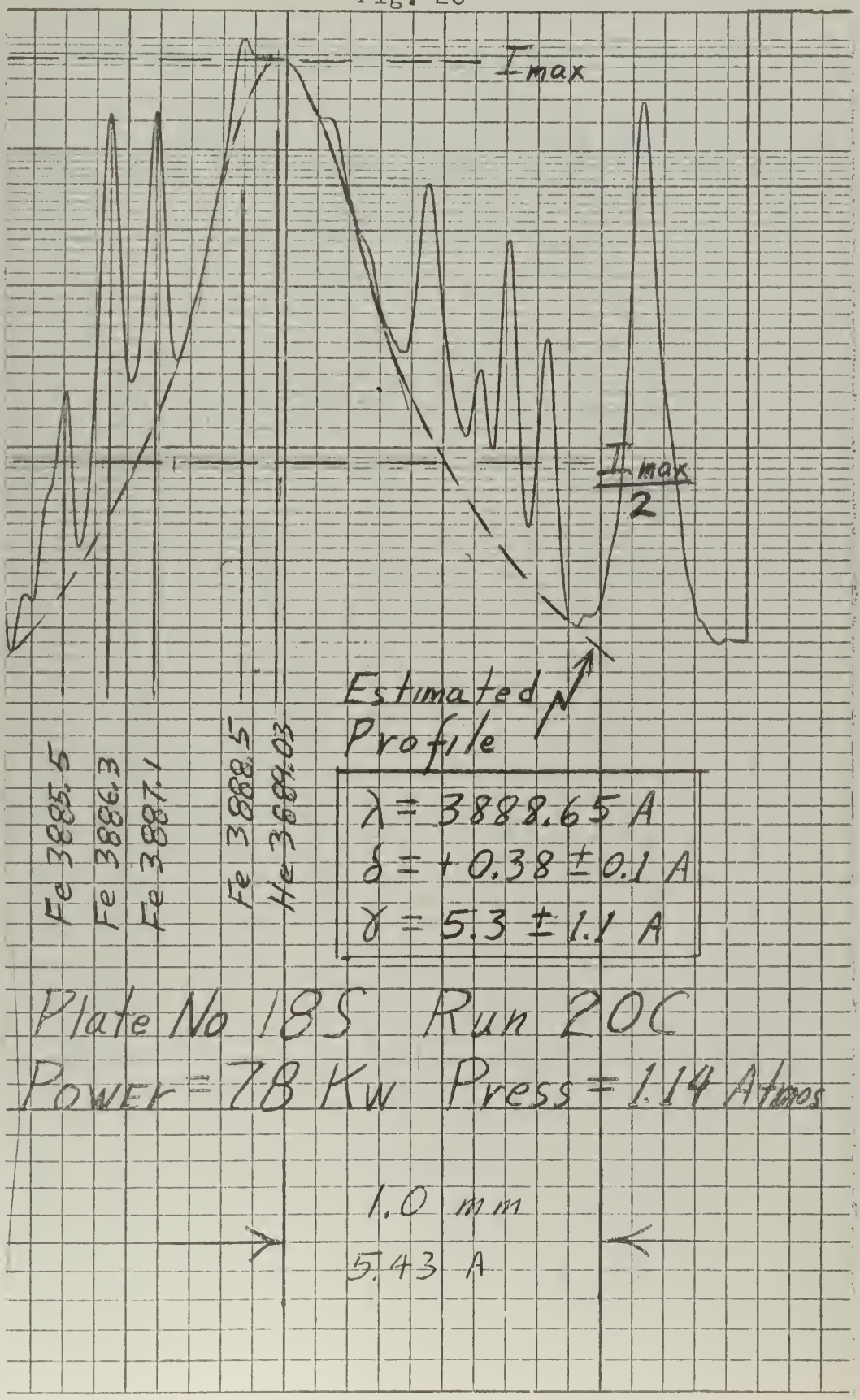
Imax
Imax/2
Fe 3885.5
Fe 3886.3
Fe 3887.1
Fe 3888.5
He 3889.03
Estimated Profile
λ = 3888.65 A
δ = +0.38 ± 0.1 A
γ = 5.3 ± 1.1 A
Plate No 185 Run 20C
Power = 78 Kw Press = 1.14 Atmos
1.0 mm
5.43 A

Fig. 21

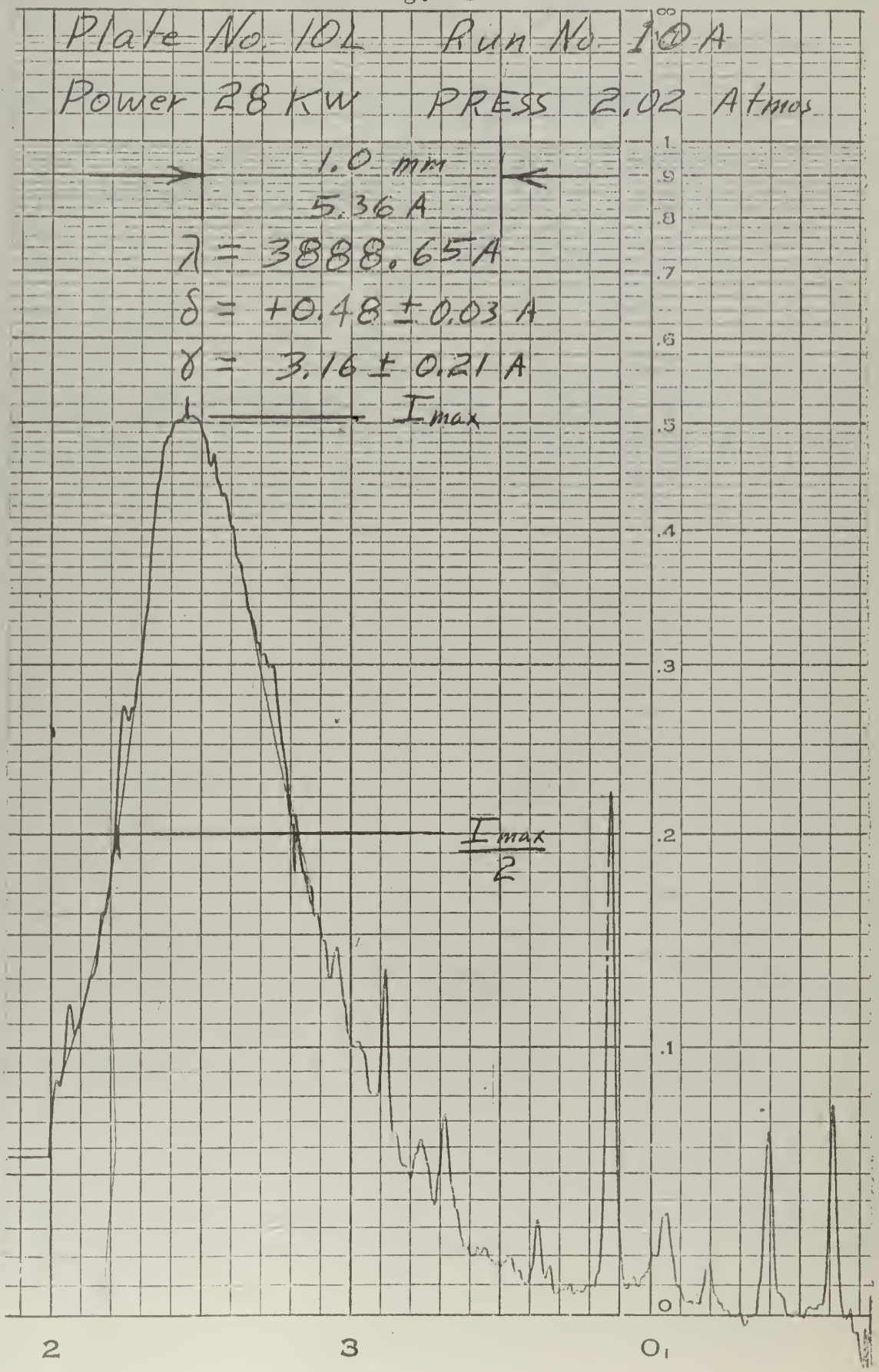
Plate No. 102 Run No. 10A
Power 28 KW PRESS 2.02 Atmos
1.0 mm
5.36 A
λ = 3888.65 A
δ = +0.48 ± 0.03 A
γ = 3.16 ± 0.21 A
Imax
Imax/2
1.0
.9
.8
.7
.6
.5
.4
.3
.2
.1
0
2
3
O1

Fig. 22

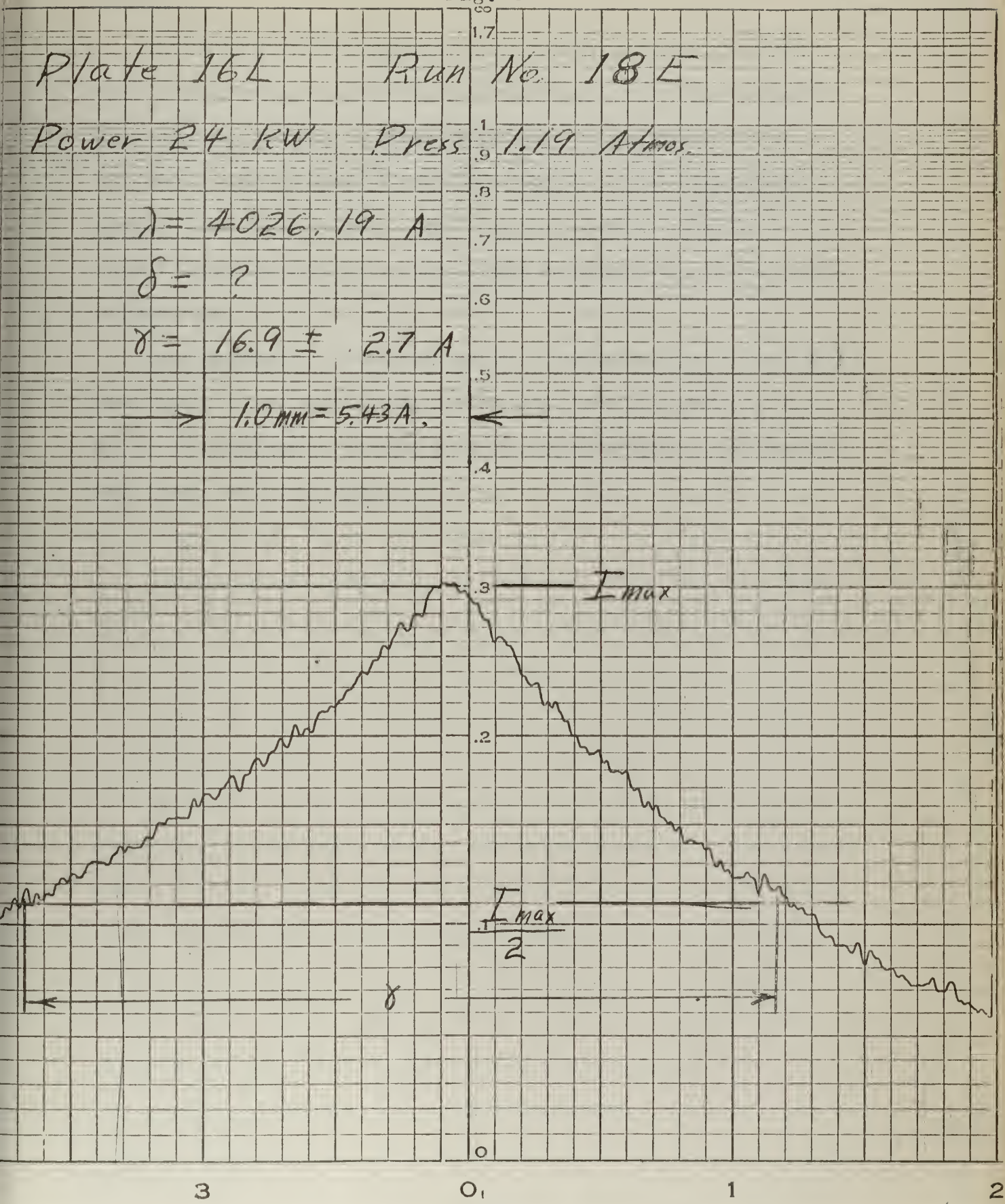
Plate 16L
Run No. 18E
Power 24 KW
Press 1.19 Atmos.
λ = 4026.19 A
δ = ?
γ = 16.9 ± 2.7 A
1.0 mm = 5.43 A.
I max
I max / 2
γ
∞
1.7
.1
.9
.8
.7
.6
.5
.4
.3
.2
.1
0
3
0
1
2

APPENDIX

The purpose of this appendix is to detail the areas of difficulty associated with the set-up and operation of the experiment for future users. Moreover a large expenditure of work and time was involved in solving these difficulties and it is hoped that this appendix will allow others to profit by the authors' experience. In certain cases, specific instructions will be given because they exist no where else.

Very generally, it will consist of three parts, one section will cover the arc jet, another the spectrograph and its operation, and lastly a miscellaneous section covering instrumentation, photographic techniques, data reduction, etc.

A. ARC JET

The physical make up, dimensions and wiring of the arc jet are included in reference 10. However, certain modifications were made to improve operation.

First, the wiring was changed to include a ground on the negative side of the circuit. Also in this change was the placing of the resistor bank and the inductance in the positive side to remove the starting and stopping transient effect on the ground. A permanament current limiting resistor, in place of the parallel resistor bank, was used in the DC motor-generator armature circuit for starting. The effect of this change was to prevent the parallel resistor bank from being above ground potential when the motor-generator was used as a generator and with the switches open.

The mechanical alterations though minor were important. Foremost was the shortening of the length of the anode inserts and that part of the anode holder and nozzle which projects into the body. The total shortening came to approximately 1/2 inch and was needed to bring the entire arc into view of the upper window. The insulating sleeve of the cathode holder was lengthened to reduce the possibility of arc-over to the body. A press fit of the sleeve was used to eliminate a retaining ring. The inside bottom of the arc jet was covered with a 1/8 inch thick asbestos ring to reduce arc-over possibility and to protect the base plate from corrosive damage. The complete set of the arc jet working drawings with alterations is in the custody of Dr. R. M. Head of the U. S. Naval Postgraduate School.

An attempt was made to calibrate the pancake coils used for magnetic stabilization. The installation of all six coils is straight

forward, one merely matches corresponding numbers on the parts. There are several traps to be avoided.

1. The pancake coil feed tubes must be insulated from the body. The use of Teflon tape is mandatory here, because of its extreme thinness and good insulating characteristics. Care must be exercised in inserting the tubes to prevent scratching through the Teflon.

2. Aircraft hydraulic hoses should not be used to carry cooling water to the coils. These hoses have a braided metal layer which can short the circuit, resulting in hose burn-out, loss of cooling water and damage to the pancake coils.

3. While reference 10 states that the number of coils may be varied, it should be pointed out that the method of attaching the electrical connections will have to be modified depending on the number of coils used.

Recommended design changes are mostly concerned with the anode holder, inserts and associated cooling. There is one exception. This is the addition of a supersonic test section This is a major design change and will not be considered here, but should be kept in mind for future development work.

The anode design should be covered by a complete report; the authors whish only to point out certain facts. There are three basic factors that should be considered, they are:

1. Simplicity. This factor would give ease of installation and reduce manufacturing complexity and time (e.g. remove present threads on anode inserts and use a forced slip fit). Carbon, high density type, is preferred for manufacturing ease and low

cost.

2. Electrical. The design should have large surfaces to reduce contact potential, particularly with carbon. Parts should have sufficient cross sectional areas to prevent high current densities and drop of potential, extremely important with carbon.

3. Cooling. The entire anode should be cooled for use at very high powers. The present design is very vulnerable to cooling failure if arc-over should occur. Adequate cooling would also prolong the life of the anode inserts.

The following cross sectional sketch (not to scale except for outside dimensions) is a suggested solution for anode design that could easily convert the apparatus from a free jet to a supersonic test section.

The mechanics of starting and operation of the arc jet remain as given in reference 10. However, the graphs of Volt-Ampere Characteristics in reference 10 must be used as only a general guide to the desired operating point. The authors found that variation in gas type, electrode material and gap spacing greatly affected the location of the operating point. Therefore, it is recommended that future users run calibration checks to determine operating points before taking data. An example of what is meant is: When using carbon and nitrogen gas large variations of external resistance and gap spacing produced very little change in current. When other gases (argon and helium) were used with the carbon electrodes, more significant changes were noted in the current when the external resistance was varied, although not as great as the tungsten-helium combination.

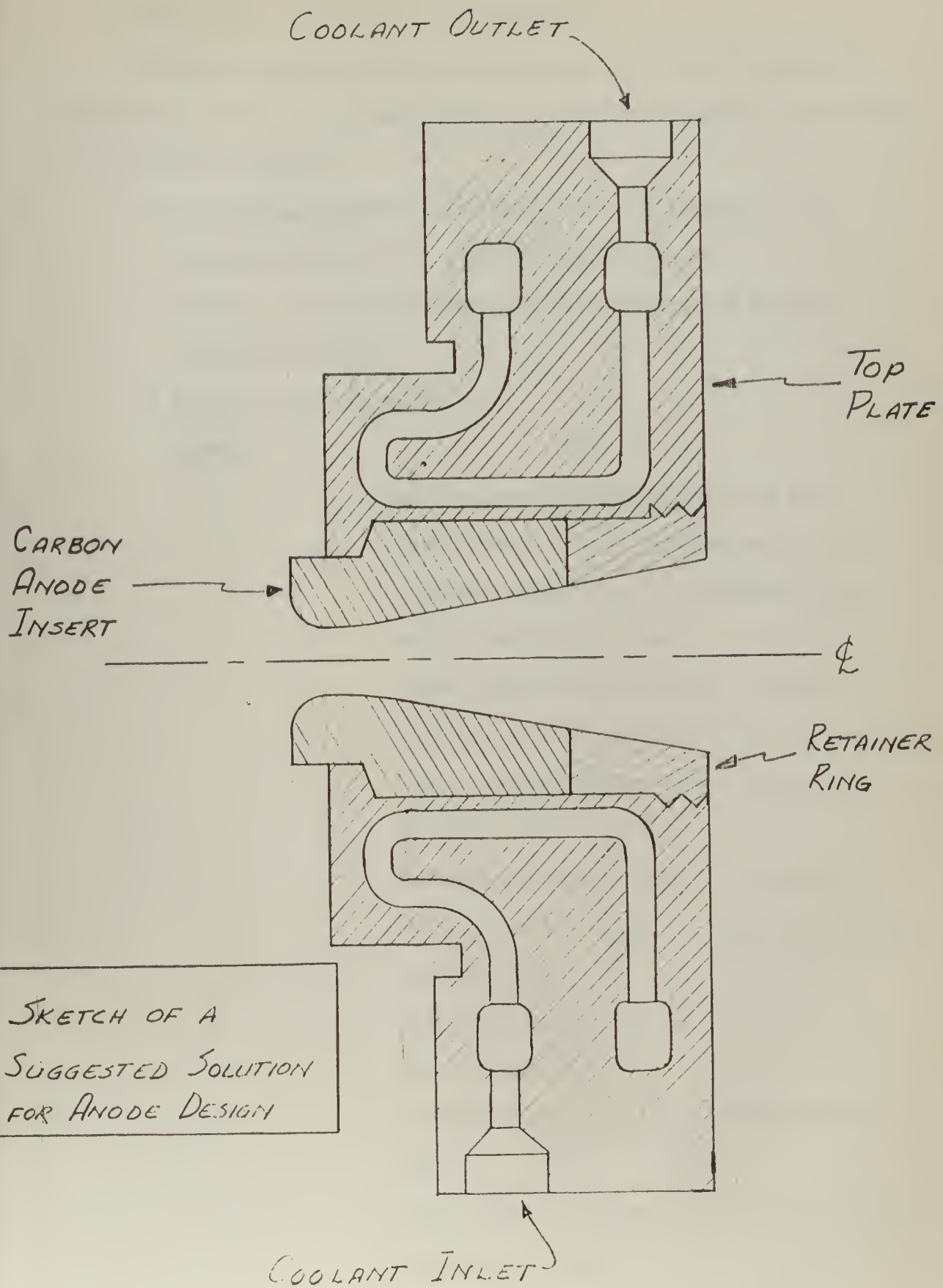

SKETCH OF A SUGGESTED SOLUTION FOR ANODE DESIGN

B. SPECTROGRAPH: CALIBRATION AND OPERATION

The spectrograph is a Baird Atomic three meter grating spectrograph, model GX-1, on an Eagle mounting. The spectrograph is comprised of the following parts.

(1) The grating and mount enclosed in a metal cabinet on a movable stand and with attached optical bench.

(2) Controls, recording mechanism and power supplies housed in a metal cabinet.

(3) The following accessories

Quantity	Item
1	Spectrographic plate camera 4" x 20".
1	Direct Reader head, complete with 5 photomultiplier tube sockets, brackets, wiring and two mounting screws.
4	1-P28 Photomultiplier tubes, serials: 28-1848, 28-1585, 28-1559, 28-1570.
3	1-P21 Photomultiplier tubes, serials: 21-788, 21-844, 21-828.
2	Sockets, photomultiplier tube (extras)
9	Exit slits, 4 - 25μ, 4 - 50μ, 1 - 150μ, 1 off-set slit.
2	Mirror mounts, exit slit.
2	Mirrors, exit slit.
4	Diffuser plates, quartz, photomultiplier tube.
5	Blue filters, photomultiplier tube, 2 thin, 2 medium, 1 thick.

1	Combination blue filter and diffuser plate, photomultiplier tube.
5	Spinner plates, #1 - 1/2 mm, #2 - 2 mm, #3 and #4 - 4 mm, #5 - 8 mm. (nominal thickness)
2 sets	Adapters for exit slit adjustment cables on DR head, 1 long pair, 1 short pair.
1 set	Entrance slits, 1 - 10 μ, 1 - 25 μ, 1 - 50 μ, 1 - 75 μ, plus fishtails for each.
1	Filter and rectangular lens holder.
1	Step filter (7 steps) and frame.
1	Hartmann diaphram.
1	Rectangular lens, 35 cm, fused quartz
2	Lens, 25 cm, Fused quartz (1 in ring holder).
1	Pinhole.
1	Plane mirror and holder.
1	External shutter, split action.
1	Hg servo lamp.
4	Optical bench saddle mounts, 2 small, 2 large.
1	Calibration card, framed.
1	Power supply for Geisler tubes plus assorted tubes.
2	Dividers, 1 small, 1 very large.
2	Metric rules, 1-10 cm, 1-50 cm.
1	Measuring magnifier, Bausch & Lomb, metric

and inch scales.

1 set — Allen keys.

1 box — Fuses, assorted.

Miscellaneous hardware

2 boxes — Envelopes, spectrographic plate.

1 — MIT Wavelength Tables.

1 — "Experimental Spectroscopy" by Sawyer.

1 — "Chemical Spectroscopy" by Brode.

1 — Handbook, spectrograph, 3-ring binder.

A three ring binder handbook is kept which contains all information pertinent to the operation and calibration of this spectrograph. This section is intended as a supplement to this file and will describe the operating techniques and calibration data obtained during the first six months use of this instrument.

1. Optical Bench

Contrary to the manufacturers description, the optical bench scale is not calibrated with respect to the slit. The following corrections must be used:

a. Scale zero to slit = 7.80 cm.

b. Step filter holder off-set =-17.0 cm.

c. Total Sirk's focus correction = 9.2 cm.

Example: To set the step filter or Hartmann diaphragm in the Sirk's focus for a grating angle of 4° and a wavelength of 4200 A.:

a. Enter the Sirk's focus graph and find the slit-to-focus-distance of 11.6 cm.

b. Add the correction; 11.6 / 9.2 = 20.8 cm.

c. Set the filter holder bench mark on 20.8 cm on the optical

bench scale.

Three fused quartz lenses as described above have been provided for use on the optical bench. These should be aligned virtically to coincide with the optical axis of the instrument which is located 8.0 inches (20.32 cm) above the top surface of the optical bench. The purpose of the rectangular lens (this is not a cylindrical lens) is to integrate the light passing through the step filter so that all parts of the step filter contribute to the line intensity. It has been found that the use of the lens- step filter combination produces the following unsatisfactory results.

a. The line of demarkation between the steps is not defined.

b. The line intensity within each step is not uniform.

The above errors may be due to a horizontal density variation in each step and/or the slight density gradient observed within each step during the microdensitometer step filter calibration.

The vertical positioning of the step filter holder was performed as follows: The Hartmann diaphragm #2 was inserted and the plate mask set at the narrowest setting. The light source, lens, or mirror was then adjusted so that the spectral lines showed a maximum intensity and were centered in the plate mask opening. This procedure proved satisfactory for most exposure identifications, but when the step filter was substituted for the Hartmann diaphragm, the image was not centered in the mask opening. (When the mask was set at 10 mm, two steps are blocked from the plate.)

In general, the technique suggested by the manufacturer of focusing the source on the grating was found to be unsatisfactory for most applications. Focusing on the grating allows for the use of the entrance

slit fishtail diaphragm to reduce the speed of the spectrograph. The amount of light passing through the slit however, is then dependent not only on the image intensity but also on the position of the source. The Geisler tubes, for instance, provided such a low intensity and were so out of focus at the slit, when mounted on the optical bench, that very long exposures were required (15-20 min.). When the tubes were focused on the slit these times were reduced to 1 to 2 min. This technique is then recommended only where intensity is no problem, maximum uniformity in line intensity is required, and standard set-ups are used, such as the use of a tungsten ribbon lamp for density calibration.

2. Grating angle, focus, and tilt.

The type of mounting of a spectrograph determines the operations required to change the wavelength region photographed by the camera. The basic operations required for the Eagle mounting used by this instrument are described in most standard texts on spectroscopy. (e.g. Sawyer, Experimental Spectroscopy) In this instrument the required motions of the grating and camera are obtained by the motions of motor driven jackscrews. The component positions are indicated by Veeder-Root counters located on the front operating panel. The counter calibrations were performed by the manufacturer and are indicated in the accompanying table. The calibrations were performed as follows: Exposures were made at various settings of focus and tilt for each degree of grating angle from 1° to 10° and each five degrees from 10° to the maximum. The exposures were then examined and the proper values chosen which produced a sharp image across the entire camera. Interpolations were then made for the intermediate points (above 10°) and the table prepared. This procedure was checked for three data points

CALIBRATION DATA FOR
3-METER GRATING SPECTROGRAPH - GX1-144

Naval Post Graduate School
Monterey, California

Degree	Tilt	Grating	Focus	Wavelength Range
1	956.4	999.0	491.5	1280 - 4120
2	953.0	998.0	490.7	1870 - 4705
3	949.0	997.0	489.5	2460 - 5285
4	944.5	996.0	488.3	3050 - 5860
5	940.2	995.0	486.7	3640 - 6440
6	935.5	994.0	484.8	4225 - 7025
7	930.8	993.0	482.6	4810 - 7600
8	926.8	992.0	479.8	5400 - 8175
9	922.0	991.0	477.0	5980 - 8745
10	918.0	990.0	473.6	6560 - 9315
11	913.2	989.0	470.0	7135 - 9880
12	909.4	988.0	465.8	7710 - 10440
13	904.5	987.0	461.6	8290 - 11000
14	900.6	986.0	456.5	8860 - 11550
15	895.2	985.0	451.7	9430 - 12100
16	890.8	984.0	446.0	9990 - 12640
17	886.4	983.0	440.3	10550 - 13180
18	882.0	982.0	434.0	11110 - 13720
19	877.6	981.0	427.5	11670 - 14260
20	873.3	980.0	420.5	12230 - 14800
21	868.8	979.0	413.0	12780 - 15330
22	864.3	978.0	405.3	13320 - 15850
23	859.7	977.0	397.5	13860 - 16370
24	855.1	976.0	389.5	14400 - 16890
25	850.5	975.0	381.2	14930 - 17390
26	846.1	974.0	372.5	15460 - 17890
27	841.7	973.0	363.6	15980 - 18390
28	837.3	972.0	354.6	16500 - 18890
29	832.8	971.0	344.5	17010 - 19380
30	828.2	970.0	334.0	17520 - 19860
31	823.8	969.0	324.0	18020 - 20320
32	819.4	968.0	313.7	18520 - 20790
33	815.0	967.0	302.6	19010 - 21250
34	810.6	966.0	291.1	19500 - 21710
35	806.2	965.0	279.3	19980 - 22170
36	801.8	964.0	267.3	20460 - 22630

after delivery and no disagreement with the table was observed. To set the spectrograph up for a grating angle not listed in the table e.g. 1.7° the following procedure has been developed (as suggested by the factory representative, Mr. Austen O'Malley): An interpolation graph has been prepared on a chart 2' x 3'. This chart is not included in this report due to its size. To use this chart, first select the wavelength region of interest. The following formula has proved of value here;

$$n\lambda_n = m\lambda_m$$

where n and m are integers which represent orders of diffraction. This formula represents all the wavelengths which will appear at the same position on the plate. For example, the following wavelengths will all appear at the same position 12,000 (1st), 6,000 (2nd), 4,000 (3rd), 3,000 (4th), 2,400 (5th), etc. These will not all be photographed however due to a ten to one reduction in intensity in each succeeding higher order, the absorption of air and glass, and the spectral sensitivity of the emulsion.

When the wavelength region of interest has been selected, the chart is entered at the left side with the center camera wavelength. Then proceed horizontally to the curve marked "wavelength". Reflecting vertically downward read grating angle (or counter reading) from the lower abscissa. Proceed vertically (up or down) to the adjacent curve marked "focus". The proceed horizontally to the curve marked "Tilt". The coordinates of this point then give focus counter reading on the right margin scale and tilt counter reading on the upper scale. Note that there are two sets of curves on the chart: One for grating angles

less than ten degrees, and one for grating angles more than ten degrees. The grating focus and tilt readings are then set up on the counters of the instrument. The correct reading is always approached from higher numbers. On approaching the desired reading, flip the switch to provide momentary contact only. This will allow for accurate setting.

3. Rack Calibration.

This section describes the relative position of the plate and the exit mask centerline. It should be noted that the position of the image relative to the exit mask will depend on the entrance optics and is described in section B. 1. above. We define the reference line as the horizontal centerline of the exit mask. This line is fixed relative to the spectrograph frame and the position of the exposure is determined by the vertical (rack) position of the plate. The camera accepts two 4" x 10" glass spectrographic plates. The camera is built with a slight end play so for consistency the plates should be butted together in the center and against the right edge of the camera. When mounted in this manner a strip 3.8 mm wide on the top and bottom of the plates will be covered by the focal plane cam. In addition, a strip 4.8 mm wide on the right edge will be covered by the camera housing. With the above configuration, the rack counter calibration is as follows: The reference line first "sees" the plate above the lower cam for a counter reading of 9780. The reference line last sees the plate below the upper cam for a counter reading of 8810. The rack counter is calibrated to read directly in tenths of millimeters so that a counter reading of 9524 would place the reference line 25.6 mm above the lower cam or about one inch up on the plate. Limit switches are provide to prevent over-driving the rack motor. These limit switches

are positioned as follows: upper limit, static-9896, dynamic-9944; lower limit, static-8877, dynamic-8866, where the difference between static and dynamic is the overshoot due to inertia. In this connection it should be noted that the overshoot can be expected to increase with time as the parts wear in. For this reason the upper limit has been set so that the dark slide is not fully seated when the plate is racked to the top. Hence the dark slide must be seated by hand before removal from the spectrograph. The up and down rack speeds are not the same. The up rack speed is 3.74 mm/sec and the down rack speed is 1.93 mm/sec. These are steady state values, which are reached after approximately 1.2 seconds of operation. (decrement of 0.63 sec^{-1})

In addition to the manual rack mode, there is an automatic mode. When operating in this mode the rack motor is started by actuation of the RACK button and stopped by the opening of a microswitch located on the rack drive shaft. It should be noted that a 2.5 mm automatic rack provides room for a 2.5 mm exposure by actually racking 3.0 mm. In the same manner, the 5.0 mm automatic rack actually racks 6.0 mm. The automatic rack mode provides the easiest way to obtain reproducable rack settings.

C. INSTRUMENTATION

As orginally conceived the instrumentation system was one of extreme sophistication where all the measured parameters; pressure, voltage, current, timing marks, exposure length, and the photomultiplier tube outputs of the spectrograph direct reader head, when used, would simultaneously and automatically be recorded by a 14 channel Ampex tape recorder, model FR-100. The instrumentation system was to have been energized by the light of the arc jet when started. In addition, they could have been annoted by voice during the run. Thus the chore of data taking would be done effortlessly. This system was actually built by the authors, but it never functioned properly or completely at any time. Most failures could be attributed to the electronic units holding the system together; however, noise was also troublesome due to the low level of the inputs. In fact, the authors had great difficulty to keep from being mesmerized by the idea of instrumentation.

The final instrumentation was much simpler than that which was envisioned. The same primary parameters, pressure, voltage, and current were measured but they were only displayed by pen recorders. The tape recorder was eliminated due to the aforementioned noise.

Each parameter's measurement will be discussed individually. The spectrograph and its components will be treated in a separate section.

1. Voltage.

The voltage was tapped as a potential above ground on the positive side of the arc (Fig. 2). The signal was amplified by an Edin amplifier, model 8105, and displayed on one channel of an Edin six channel pen recorder. Pen deflection was generally calibrated for 0.2 mm/volt.

2. Current

The current was proportional to the output of two transductors. A complete statement of the theory which governs the operation of the transductors used to measure current is beyond the scope of this report. It may be found in any standard reference on magnetic amplifiers. Essentially the transductor operates as a direct current transformer by maintaining the equality of ampere-turns between the control winding (the single turn formed by the bus passing through the center of the device) and the load winding. To measure the current in a bus, the bus is passed through the central hole in the device and a 60 cycle voltage is applied to the load winding. The current in the load winding is then rectified with a full wave rectifier (silicon diodes) and the rectified current measured with a D.C. ammeter. For bus currents between 2% and 100% of the rated transductor current, the metered current is proportional to the bus current. The constant of proportionality is determined by the number of turns in the load winding. The following transductors, manufactured by the Control division of Magnetics, Inc., were used:

Type 4303, 120 volts, 60 cycles, nominal bus current 1000 a., current ratio 1000/0.2,

Type 4327, 240 volts, 60 cycles, nominal bus current 5000 a., current ratio 5000/2.

The rectified currents were amplified by Edin amplifiers, model 8105, and displayed on two channels of the Edin pen recorder. Pen Deflection was calibrated for 200 amp/mm.

3. Pressure.

The gage pressure in the arc barrel was detected by various

Wiancko variable-reluctance pickups. The pickup signal modulated a Wiancko frequency modulated oscillator, model 18-1308. Since the range of the oscillator is 2 kc, the 0-200 psig pickup was used more often for simplified calibration. The FMO analog output was recorded by the Edin system. The FMO-HI output was connected to a Hewlet-Packard electronic counter, model 523B, and thence to a Hewlet-Packard Digital Recorder, model 560A for print out. The counter was used primarily for the calibration of the pickup and FMO for a specified pressure range using a dead weight tester.

4. Miscellaneous.

Timing intervals of one second as well as the duration of the spectrograph exposure were displayed by the pen recorder.

The exposure length was timed by a General Electric electronic timer, model CR 7504, which was tied to the spectrograph automatic shutter. The timer was connected into the circuit using the EDE mode of operation. The spectrograph's automatic shutter leads were connected across terminals 6 and 8 and the marker pen motor across terminals 3 and 7. The horizontal sweep of a Tectronic oscilloscope, model 545, was used to calibrate the exposure length. The shutter switch on the spectrograph must be in automatic for operation.

To obtain the data for a run, it was only necessary to turn on a master switch to energize the pen recorder since all amplifiers were on continuously to minimize drift. The exposure timer was actuated by a separate switch at the appropriate time during the run.

The camera used for the color movies was a Bolex H-16. All film was exposed using the telephoto lens.

The Edin amplifier-pen recorder system was used for its rapid

response. The system becomes non-linear with approximately 1.2 cm of pen deflection from the undeflected position. This non-linearity varies with

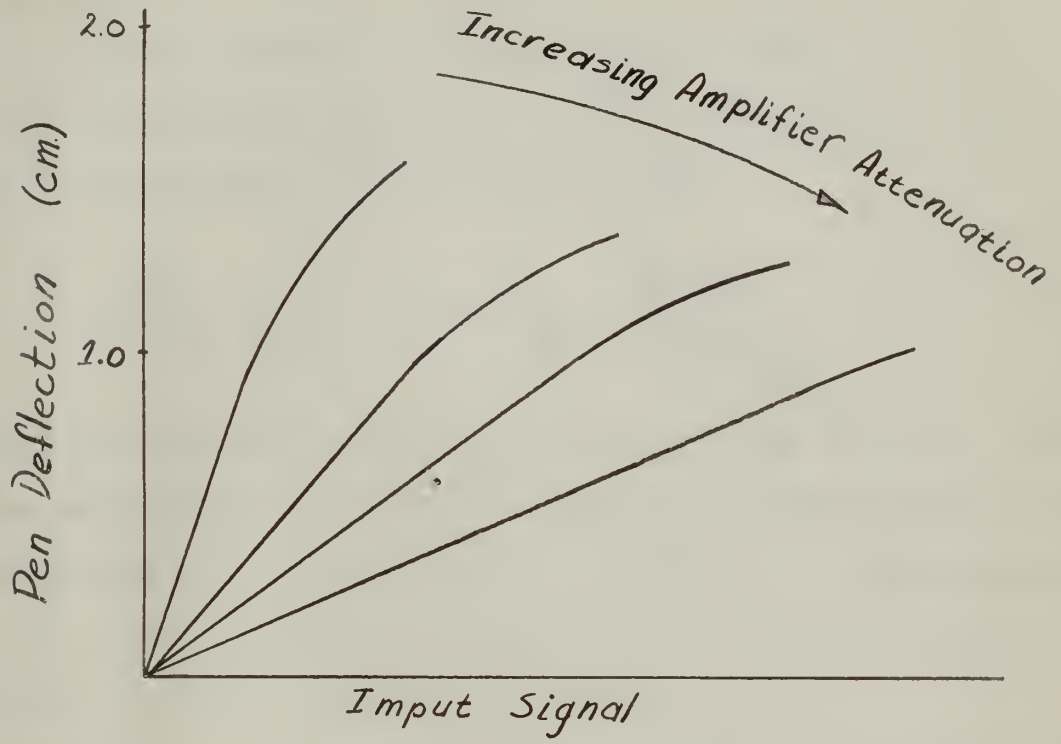

input signal magnitude, amplifier attenuation setting and the pen motor - amplifier combination used. Thus, it is imperative that the Edin system be calibrated for expected inputs.

D. STEP FILTER CALIBRATION

The step filter as supplied with the spectrograph was uncalibrated although the nominal intensity ratio per step was listed as 2:1. Two methods were tried for step filter calibration. One consisted of making microdensitometer tracings of the filter and using the following relation for the intensity ratio:

$$D_n - D_{n-1} = \log I_n / I_{n-1}$$

where D is the density from the tracing and I is the intensity. The other method consisted of passing light from a tungsten ribbon lamp through each filter step, while mounted sideways on the spectrograph optical bench, and measuring the intensity with the photomultiplier tubes of the DR head at various wavelengths.

The results of the calibration attempts and the step widths are listed in the following table. The microdensitometer method gives an average or integrated value for the ratio.

When using the step filter the table is entered with the wavelength closest to the region under consideration for the intensity ratio. In actual practice the delineations between steps was so fuzzy on the spectrographic plates that threads were placed on two of the step boundaries. The step filter must not be used next to the lens as noted in section B. (1).

STEP FILTER CALIBRATION

Step Number	Step Width (mm)	I_n / I_{n-1} #	I_n / I_{n-1} ★ 3635 A	I_n / I_{n-1} ★ 3889 A	I_n / I_{n-1} ★ 4200 A	I_n / I_{n-1} ★ 4686 A
No Filter		1.08				
1	3.0	1.41	1.50	1.51	1.45	1.60
2	1.4	1.52	1.53	1.55	1.59	1.42
3	1.3	1.53	1.53	1.69	1.64	1.89
4	1.3	1.48	1.51	1.43	1.55	1.59
5	1.5	1.515	1.67	1.76	1.65	1.69
6	1.3	1.38	1.36	1.61	1.61	1.30
7 (Densest)	2.7					

Microdensitometer tracing.

★ Photomultiplier tubes.

E. PHOTOGRAPHIC TECHNIQUES

The wavelength region to be studied determines the general category of spectrographic plates to be used. Particular attention must be given to the plate cut off at the longer wavelengths. Within each category there is a choice of emulsion speeds. Fast emulsions, which usually have low contrast, are undesirable because large variations in intensity produce only small variations in density. On the other hand, plates having very high contrast (slow speed) can be used over only a narrow intensity range, and one is likely to find it necessary to work with over and under exposed portions.

Exposure times varied according to the method of focusing the arc jet. If the arc jet was focused on the spectrograph slit then exposure times varied from 0.2 to 1 sec. for SA-1 and SA-2 plates. If the arc jet was focused on the grating then exposure times were as long as six seconds. The determination of exposure times is primarily a matter of practice and experience.

Precise darkroom techniques are a must. New developer (D-19) must be used for each set of plates. The necessary formulae, times and other information for proper development are given in Kodak's "Materials for Spectrum Analysis". All texts recommend brushing the plates during development to reduce the Eberhard effect. The authors found that a small viscose sponge performed this task suitably. Finally the plates must be allowed to dry in a dust free area.

A system for identification and indexing of plates should be decided upon and used at all times. Identification of right and left plates and the center edge are items to be included in the system. Exposures must be properly spaced to allow room for line annotation.

Regardless of the type of plate used, all emulsions, even from the same box react differently to light intensity. Since spectral theory (line broadening, etc.) usually involves intensity of the emitted light and spectrographic plates record density, there must be a correlation between the two for each plate. This takes the form of a curve plotted for Density vs. log Intensity. The step filter is used to give changes of density on the plate and for this reason the step filter intensity ratios must be known. Iron spectrum, in conjunction with the step filter, was used to provide the necessary data for each emulsion calibration following the precautions listed in the above Kodak handbook.

The user should become familiar with the above handbook and its references plus a text on spectroscopy, such as "Practical Spectroscopy" by Harrison, Lord and Loofbourow, for the complete photographic procedures.

SERVO PATTERNS

NO EXIT SLIT

SPINNER ON

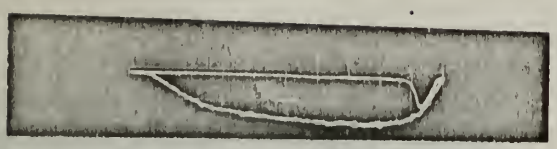

Sine sweep

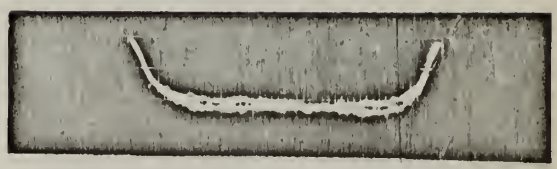

Incorrect lamp - scope phasing.

Correct lamp - scope phasing.

Linear sweep

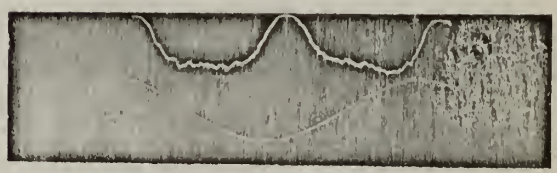

top - lamp output

bottom - line voltage

NO EXIT SLIT

SPINNER ON

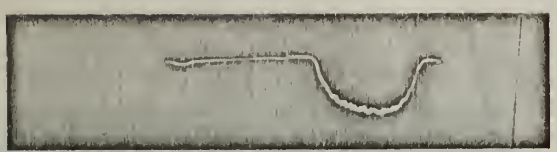

Linear sweep

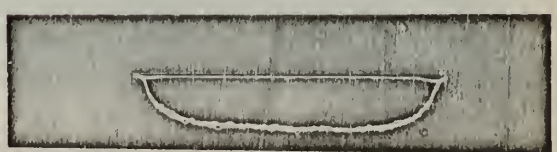

Sine sweep

Correct spinner - scope phasing

NO EXIT SLIT

SPINNER ON

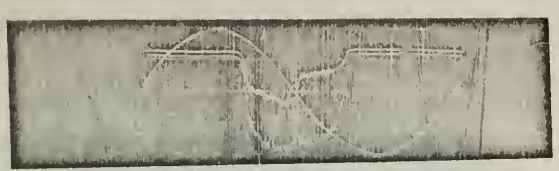

X & Y OVER and LINE

Linear sweep

Sweep mag. = X1

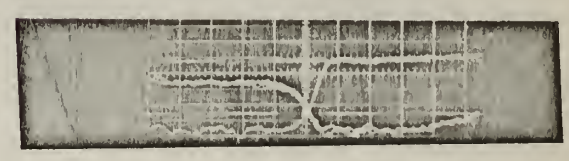

X & Y OVER and SCOPE CAL OUT

Linear sweep

Sweep mag. = X1

X - OVER PATTERN ADJUSTMENT

Note: Scope photographs are double exposures, one exposure on phase A and one on phase B.

INCORRECT

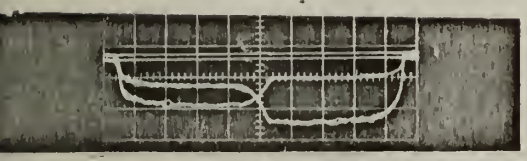

Without trimmer bar.

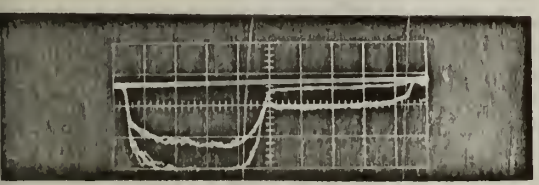

Trimmer bar misadjusted.

CORRECT

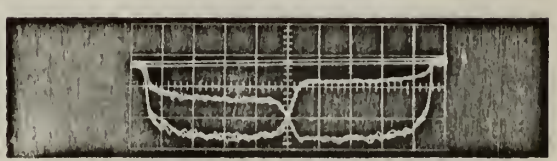

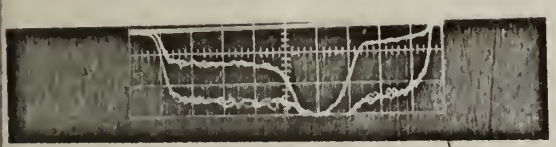

Slit tilted.

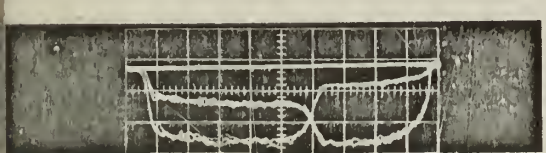

Slit off center.